

DEM simulations of vibrated sphere packings in slender prismatic containers



Sujith Reddy Jaggannagari ^{a,1}, Raghuram Karthik Desu ^{b,1}, Jörg Reimann ^c, Yixiang Gan ^d, Marigrazia Moscardini ^e, Ratna Kumar Annabattula ^{a,f,*}

^a Department of Mechanical Engineering, Indian Institute of Technology Madras, Chennai 600036, India

^b Department of Mechanical Engineering, National Institute of Technology, Tiruchirappalli 620015, India

^c Institute for Applied Materials, Karlsruhe Institute of Technology, 76344 Eggenstein-Leopoldshafen, Germany

^d School of Civil Engineering, The University of Sydney, NSW 2006, Australia

^e Department of Civil and Industrial Engineering, University of Pisa, Italy

^f Additive Manufacturing Group - Centre of Excellence in Materials and Manufacturing for Futuristic Mobility, Indian Institute of Technology Madras, Chennai 600036, India

ARTICLE INFO

Article history:

Received 14 January 2021

Received in revised form 4 June 2021

Accepted 20 June 2021

Available online 25 June 2021

Keywords:

Discrete element method

Mono-sized particles

Polydisperse particles

Packing fraction

Slender prismatic containers

Void fraction

ABSTRACT

Discrete Element Method (DEM) simulations are carried out to investigate the packing structure of the vibrated mono-sized and polydisperse particle assemblies in slender prismatic containers. Quantities like void fraction distributions, coordination number distribution, Voronoi packing fraction distributions were analyzed. DEM simulations show excellent agreement with the experimental data. The transient response of the packing structure during the vibration of mono-sized spheres reveals that the crystallization starts at the walls. The packing structure's crystallinity enhances during vibration, increasing the packing density of the assembly. Vertical vibration is found to be more effective compared to lateral vibration. The packing structure is found to be independent of the container's orientation during the filling process. The influence of the ratio of the container dimensions to mean particle diameter (X/d_m) and polydispersity (λ) on the packing structure is analyzed. The results showed that the increase of X/d_m ratio or λ , increases the random arrangement of particles.

© 2021 Elsevier B.V. All rights reserved.

List of symbols

Bulk material properties

E Young's modulus

ν Poisson's ratio

e Coefficient of restitution

μ Coefficient of friction

μ_r Coefficient of rolling friction

Particle and container parameters

d Diameter of the particles

d_m Mean diameter of the particles

γ_{total} Packing fraction of the total volume

γ_{lsc} Packing fraction of the large slender container

λ Polydispersity

a Amplitude of the container vibration

f Frequency of the container vibration

X, Y, Z Dimensions of the container

x, y, z Coordinate axis

Abbreviations

DEM Discrete element method

VFD Void fraction distribution

Lsc Large slender container

CND Coordination number distribution

VPFD Voronoi packing fraction distribution

1. Introduction

Granular media have increasingly become an integral part of various fields of engineering, pharmaceuticals, food processing, and the power sector. The discrete nature of granular materials leads to their complex macroscopic response. Granular systems like nuclear fusion breeder beds, electrodes in batteries, and thermal energy storage devices

* Corresponding author at: Department of Mechanical Engineering, Indian Institute of Technology Madras, Chennai 600036, India.

E-mail addresses: sujithreddyiitm@gmail.com (S.R. Jaggannagari), desu@nitt.edu (R.K. Desu), reimann-langhans@web.de (J. Reimann), yixiang.gan@sydney.edu.au (Y. Gan), marigrazia.moscardini@dici.unipi.it (M. Moscardini), ratna@iitm.ac.in (R.K. Annabattula).

¹ Equal contribution.

[1–3], undergo various thermo-mechanical interactions [4–11]. These interactions may lead to volumetric heating [12], particle breakage [13–15], and thermal expansion [16] influencing overall thermo-mechanical response of the systems. The packing structure of granular systems is shown to influence the evolution of their thermo-mechanical responses [17–22]. Therefore, the formation and evolution of the packing structure of granular systems under external stimuli is an important aspect of the study for understanding their behavior and for their better design.

Particle dynamics can be modeled using the Discrete Element Method (DEM). It is one of the efficient and widely used numerical tools to compute the motion of the particles and inter-particle interactions, simulating the behavior of granular media. Cundall and Strack [23] first introduced the formulation of the discrete element method for granular materials. DEM is typically used to model the interactions at the particle level to investigate the impact of these interactions on the whole system at a macroscopic level. In general, the packing structure of an assembly is influenced by various factors like particle container geometry, shape and size of the particle, particle bulk properties, and densification techniques. The packing of spherical particles into various container geometries such as cubical [24], cylindrical [25] and U shaped [26] have been investigated in the past. The influence of various particle shapes such as spherical [27], cylindrical [28], cubical [29], tetrahedral [30], ellipsoids [31,32], other complex shapes [33–36] and particles of varying size distribution [37] have also been analyzed through DEM simulations. DEM is extensively used to understand several aspects of granular system, and various studies like evolution of fabric and mixing of granular assemblies [38–42], determination of effective thermal conductivity of the pebble bed [43–46], and powder spreading in powder-bed based additive manufacturing process [47] have been studied in recent years.

In the past, most of the studies on packing were performed for gravity filling, achieving moderate packing fractions. However, in most technical applications, dense packing is desired. There are different densification techniques like vibration, knocking, tapping, and hammering [48,49], which result in higher packing densities compared to mere gravitational filling. Among these, vibration is the standard densification technique. With the improvement of experimental capabilities, e.g., by tomographic techniques, and the further development of the DEM techniques, extensive research was carried out on vibrated sphere packings. The experimental investigations and DEM simulations on such vibrated packings have shown that, during vibration, the disordered structure transforms into an ordered structure leading to crystallization of the assembly [24,48,50–64].

In the following, the non-homogeneous nature of particle arrangement in the finite confinements is discussed. The experimental investigation by Benenati and Brosilow [65] revealed, for the first time, the non-homogeneous nature of the packing structure from the wall to the bulk of the container. This topic is of importance for technical applications, and it has been addressed since then in many papers, see e.g., [24–26,48,54,59,60,62]. For instance, DEM simulations of packing mono-sized particles in the cubical container with consideration of gravity effect and horizontal vibration carried out by Desu et al. [24] reveal that the wall effect is seen up to few layers as shown in Fig. 1. The fluctuation of the packing fraction is due to the wall effect (near the wall) and the dampening out of fluctuations depicts the non-structured packing (away from the wall). It should be noted that these fluctuations also exist for non-vibrated particle beds, an experimental result is given in [48], and for DEM simulations with gravitational filling [24–26]. However, the fluctuations are less expressed compared to vibrated particle beds.

Regarding the results presented in the following sections, previous DEM work on the packing of particles with vertical vibration is briefly discussed. Here, work started with the development of regular structures above the bottom plate using periodic boundary conditions, see e.g., [52,57,61]. This method was extended for lateral walls for circular,

cubic, and prism-like containers [24,62,63]. Generally, the distance between opposite lateral walls was large compared to the particle diameter resulting in no interconnection of wall layers. For circular containers [62], the case of a cylinder to particle diameter ratio of 13 was investigated. Because of the circular walls, the build-up of regular structures is significantly restricted.

For the investigations described in this work, a slender prismatic container is considered, and the DEM results are compared with experimental tomography results carried out by Reimann et al. [64]. The reason for this is twofold: i) the practical importance of slender prismatic containers in the area of solar thermal energy storage systems, lithium-ion batteries, and breeding blankets in future thermal fusion reactors [10,66–70], ii) because of plane walls, no wall curvature effects exist; the wall layers at the two large opposite walls can become more easily interlinked. Such a defined geometry is also well suited for the investigation of wall structures developed in the packing of mono-sized spherical particles and polydisperse systems. The transient response of a mono-sized packing structure with vibration is also analyzed. The vital factors influencing polydisperse packing structure, like the ratio of the container dimensions to the particle's mean diameter (X/d_m ratio) and polydispersity (λ) (to be defined later), were also studied. The outline of the paper is as follows. The details of the simulations carried in this work are discussed in Section 2. The results and discussions are reported in Section 3. Further, DEM simulations on mono-sized and polydisperse packings were presented in Sections 4 and 5. Finally, Section 6 summarizes the paper.

2. Details of experimental and simulation methodology

In this section, the procedure for different simulations carried out in work is described. A slender prismatic container, used in [64] with dimensions $X = 20$ mm and $Y = Z = 80$ mm with a filler opening at top right as shown in Fig. 2(a) is used for the simulations. The walls of the containers parallel to the yz plane at $x = 0$ mm and $x = X$ are labeled as back and front wall, respectively. The walls parallel to the zx and xy planes are labeled as sidewalls (see Fig. 2(a)). The sidewall-3 (container wall at $z = 0$) is oriented at an angle 45° to the horizontal during the filling process such that filler opening is at the highest elevation as shown in Fig. 2(b). The particles are filled up to 60% of the container volume initially under gravity. Then the container is vibrated vertically along z' -direction (against the gravity direction) with amplitude 0.6 mm (0.5 times mean radius of the mono-sized particle) and frequency of 100 Hz for 15 s as shown in Fig. 2(b). Vibration is halted, and the container volume is filled up to 80% followed by the same vibration parameters as before, this process is repeated until the container is completely filled. After the final filling, the container is rotated back to zero orientation and vibrated to remove any heap formation. The above chosen dimensions of the container and the filling strategy are similar to the experiments [64]. The simulations are carried out in open-source DEM package LIGGGHTS [71] with Hertzian contact model for particle-particle as well as particle-wall interactions. The procedure followed by Reimann et al. [64], to analyze the packing structure experimentally is as follows. Hard X-rays were used to obtain the tomographic data of the assembly. Radiographic images of the assembly are taken from different angles, and tomography of the assembly is reconstructed from these images; thus, volume images are obtained. The volume images are analyzed using iMorph software [72] to get the details of spheres and contacts among them.

The mono-sized and polydisperse packings have been simulated in the present study. The particle properties and parameters used in the simulations are given in Table 1, and the simulations carried out are listed in Table 2. The results of the simulations are discussed in Sections 3 to 5.

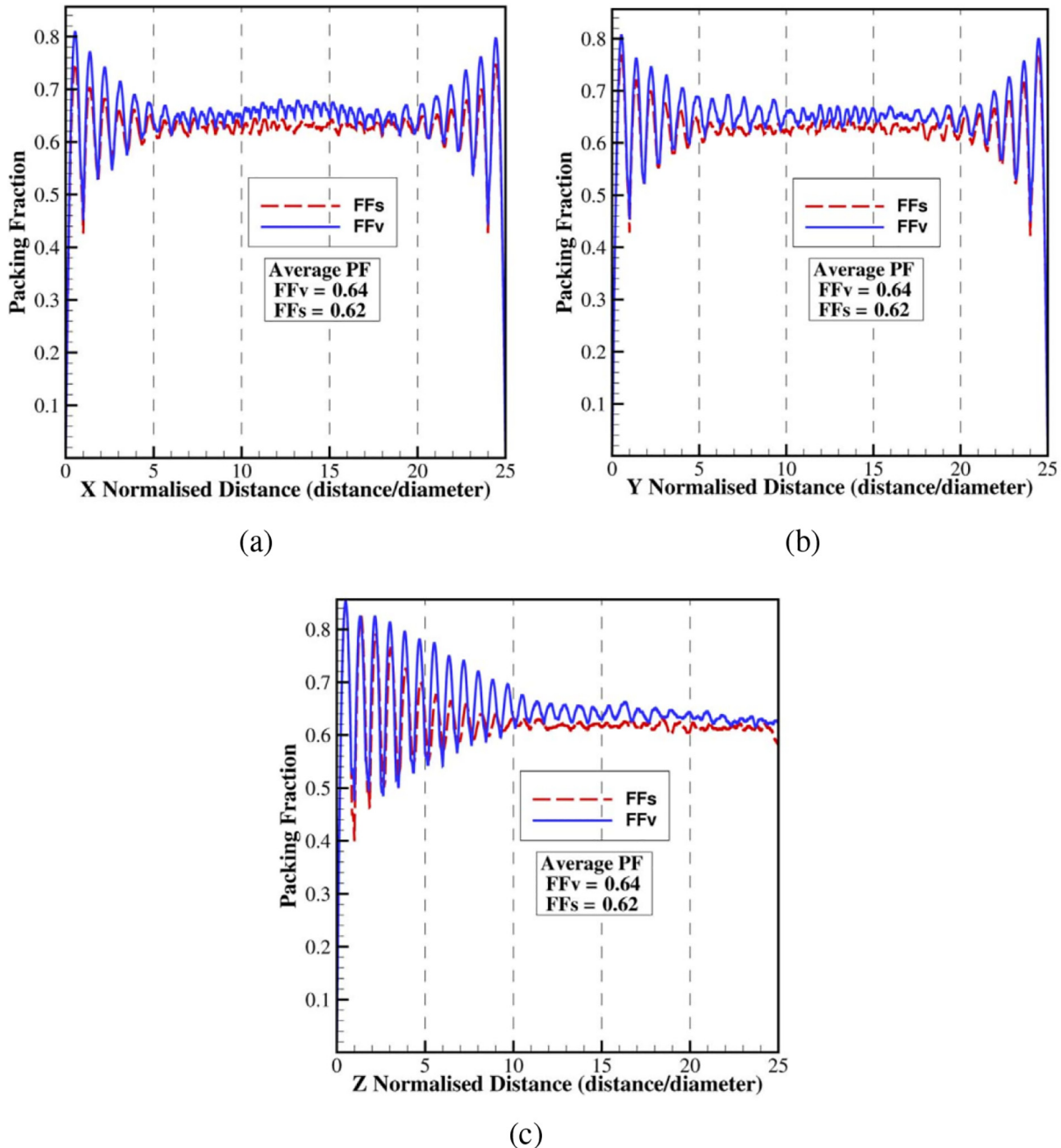


Fig. 1. The variation of packing fraction [24] along (a) x-direction, (b) y-direction, and (c) z-direction under gravity filling for laterally vibrating container (FF_v) and static container (FF_s). [Color online].

3. Validation with experiments

In this section, the results of the numerical simulations carried out for both mono-sized and polydisperse particle packings (cases SM1 and SP1 in Table 2) were compared with the experimental results [64] (cases EM and EP in Table 2). The characteristic quantities like void fraction distribution (VFD), particle distribution at the walls, coordination number distribution (CND), and Voronoi packing fraction distribution (VPFD) were used for the comparison. The different volumes equivalent to the experiments are used to calculate the above quantities are listed in Table 4. The post-processing of the data to calculate the above mentioned quantities was carried out using MATLAB [73].

3.1. Void fraction distribution

For the case of vibrated mono-sized particle assembly, a densely packed structure is observed in the simulations with a packing fraction (γ_{total}) equal to 0.675, which is close to the experimental value of 0.68. Fig. 3(a) and 3(b) show a good agreement of the void fraction distribution (VFD) for total volume and large slender container (lsc) along the x-direction for the simulated assembly and the experimental results, respectively. The large slender container (lsc) is considered to be characteristic of two infinitely large parallel plates separated by a distance of X. In Fig. 3(b) (lsc), the VFD minima are at lower values than those in Fig. 3 (a) (total volume) which result in an increased γ_{lsc} of 0.71 compared to

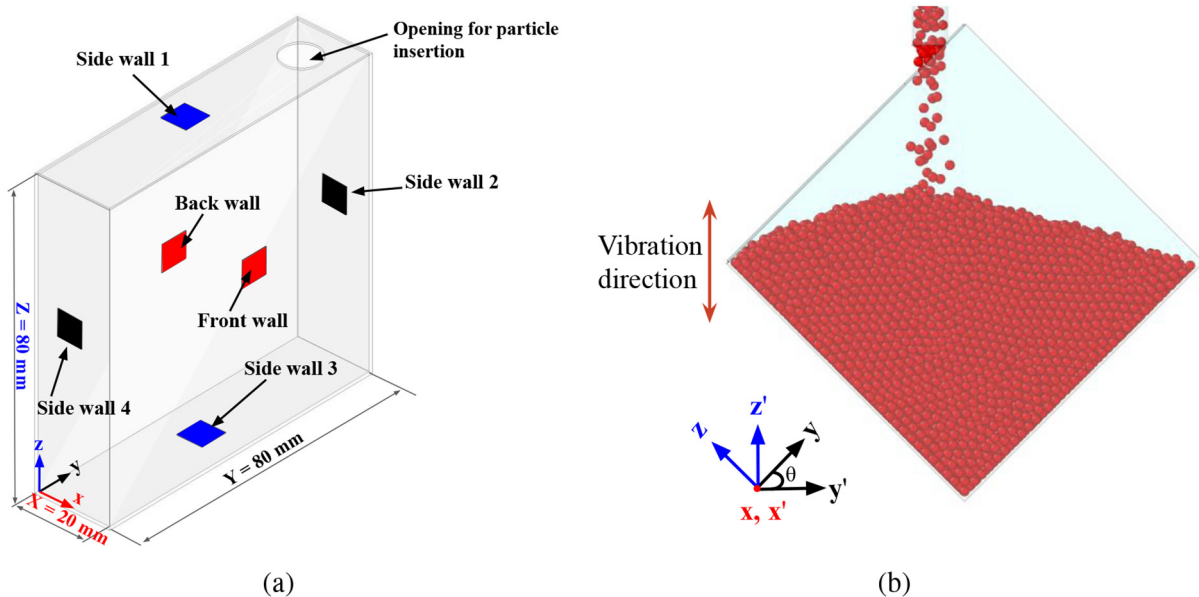


Fig. 2. (a) Schematic of the slender prismatic container used in simulations, (b) Filling of particles into an inclined container. [Color online].

$\gamma_{\text{total}}=0.675$, see Table 2. The VFD in the x-direction fluctuates from wall to wall. In prismatic containers with $X/d_m = 25$, the fluctuation zones were limited to a distance of about six pebble diameters close to the walls [24], while a larger distance is also possible with changes in geometry and vibration parameters [48]. For the slender container with $X/d_m \approx 8.33$, only ten pebble layers exist in the x-direction, resulting in the interlocking of the wall zones developing from each wall. Hence, the formation of regular dense packing is seen in the entire volume along the x-direction. The double-peaked maxima of each wave observed in Fig. 3(a) and 3(b), are a unique characteristic of dense packing, as already observed experimentally by Reimann et al. [48] in cylindrical containers. The void fraction distributions along y and z directions shown in Fig. 3(c) and 3(d), are also in good agreement with the experimental results. In Fig. 3(d), the difference in VFD near 80 mm along the z-direction is that the container is not completely filled in simulations due to numerical difficulty. Whereas in experiments, the container can be easily completely filled. Hence, along the z-direction, the VFD reaches the value of 1.0 lower than 80 mm in simulations compared to experiments. Furthermore, the higher void fraction (higher amplitudes) between experimental and numerical results is because of the relatively more ordered packing structure in simulations than experimental findings [65]. For instance, Fig. 7(a) and Fig. 7(b) depict the sphere distribution in the xy plane to be more ordered in simulations compared to experiments. The slight variation of experimental VFD along y and z directions near the walls is caused due to the lower density of the particle

at the wall. Such disturbances have not been observed in simulations, hence resulting in a similar trend (minima and maxima in VFD) throughout the volume.

For vibrated polydisperse-sized particle beds, the VFDs along x, y, and z directions, the simulation results again agree well with the experiments as seen in Fig. 4(a) to 4(d). The packing fraction obtained for the simulated assembly is about 0.623, which is slightly higher than the experimental value of 0.62. In contrast to the mono-sized packing, the VFD fluctuations damp out after 4–5 wall layers resulting in the formation of a bulk region, where the particles are no longer arranged in regular structures. Hence, interlocking of the wall effect arising from opposite walls is not observed in the polydisperse case.

3.2. Particle distribution in various planes

In this section, the distribution of spheres on different walls is analyzed. The close-packed mono-sized assembly may resemble the ideal stacking sequence of ABAB, ABCABC analogous to HCP, or FCC close packing observed in crystalline materials. Here, the ideal ABAB and ABCABC stacking have been constructed with similar dimensions of the simulation box, and the arrangement of particles at walls is analyzed and compared.

For the mono-sized assembly, Fig. 5 shows the arrangement of pebbles in the first wall layer of the front wall for simulation, experiment, and ideal (ABAB and ABCABC) cases. Formation of vertical sphere chains is observed in both simulation and experiment, resulting in a dense sphere coverage inline with the two ideal cases (ABAB and ABCABC stackings), as observed in Fig. 5. In both the ideal cases, 'A' stacking is formed as the first wall layer; hence Fig. 5(c) and 5(d) look similar. Formation of the chains, either horizontal or vertical, results in equally dense packing, as observed in experiments [64]. As both configurations (horizontal and vertical chains) are equally stable, either of them or a combination can be observed in the first layer near the wall. The walls support the creation of stable particle packing patterns, which further act as a basis for forming subsequent dense layers. Similar sphere distribution is also observed on the opposite wall (back wall). Few structural defects (voids) are observed in simulations as well as in experiments.

The distribution of particles in the first layer on the side wall-4 is shown in Fig. 6. Sphere distribution obtained by simulation (Fig. 6(a))

Table 1
Material properties and simulation parameters.

Parameters	Spheres	Container
Young's modulus, E	210 GPa	3 GPa
Poisson's ratio, ν	0.3	0.3
Coefficient of restitution, e	0.55	0.6
Coefficient of friction, μ	0.1	0.1
Coefficient of rolling friction, μ_r	0.02	0.02
Time step, δt	1×10^{-6} s	
Amplitude of vibration, a	–	0.6 mm
Frequency of vibration, f	–	100 Hz
Duration of vibration after each filling	–	15 s

Table 2Experiments and DEM simulations in prismatic containers, $Y = Z = 80$ mm.

Cases	X (mm)	Diameters (mm)	d_m (mm)	X/d_m	λ	γ_{total}	γ_{isc}	Ref
Experiments	EM	20	2.4	2.4	8.33	0	0.680	[64]
	EP	20	1.04, 1.11, 1.18	1.11	18.01	0.063	0.620	
DEM Simulations	SM1	20	2.4	2.4	8.33	0	0.675	0.710
	SM2 ^a	20	2.4	2.4	8.33	0	0.594	0.606
	SP1	20	1.04, 1.11, 1.18	1.11	18.01	0.063	0.623	0.637
	SP2	30	2.25, 2.4, 2.55	2.4	12.5	0.063	0.625	0.640
	SP3	20	2.08, 2.22, 2.36	2.22	9.01	0.063	0.617	0.633
	SP4	20	2.25, 2.4, 2.55	2.4	8.33	0.063	0.613	0.634
	SP5	20	2.3995, 2.4, 2.4005	2.4	8.33	0.00021	0.665	0.705
	SP6	20	2.399, 2.4, 2.401	2.4	8.33	0.00042	0.661	0.709
	SP7	20	2.3985, 2.4, 2.4015	2.4	8.33	0.00063	0.668	0.709
	SP8	20	2.398, 2.4, 2.402	2.4	8.33	0.00083	0.663	0.703
	SP9	20	2.395, 2.4, 2.405	2.4	8.33	0.0021	0.677	0.713
	SP10	20	2.39, 2.4, 2.41	2.4	8.33	0.0042	0.655	0.699
	SP11	20	2.385, 2.4, 2.415	2.4	8.33	0.0063	0.663	0.707
	SP12	20	2.38, 2.4, 2.42	2.4	8.33	0.0083	0.664	0.706
	SP13	20	2.35, 2.4, 2.45	2.4	8.33	0.021	0.644	0.674
	SP14	20	2.3, 2.4, 2.5	2.4	8.33	0.042	0.625	0.647
	SP15	20	2.25, 2.4, 2.55	2.4	8.33	0.063	0.613	0.634
	SP16	20	2.2, 2.4, 2.6	2.4	8.33	0.083	0.612	0.630
	SP17	20	2.1, 2.4, 2.7	2.4	8.33	0.125	0.614	0.630
	SM ^b	25	1	1	25	0		[24]

^a SM2: Mono-sized particles packing without vibration.^b SM: $Y = Z = 25$ mm.

matches well with experiment (Fig. 6(b)). It is observed that the sphere distribution is less dense on this wall when compared with the sphere distribution on the front wall. In the ideal cases, it is seen that there exists a clear close packing arrangement of particles with regular patterns (Fig. 6(c) and 6(d)). A similar regular pattern can be observed in small regions (patches) in the case of simulation, indicating particles arranging towards a more stable and close packing.

Fig. 7 shows sphere distribution on the side wall-3 for different cases. The spheres are mostly seen to arrange at a angle of 45° in simulation (Fig. 7(b)) and experiments (Fig. 7(a)), which is similar to the ideal ABCABC case (Fig. 7(d)). A slight disorder is observed in experiments and simulations, giving rise to particles' arrangement at supplementary angles, as each one arises from the walls and propagating inwards and intercepting each other. The ABAB wall structure (as shown in Fig. 7(c)) seems to differ from the remaining cases. The particles in the ABAB case have also arranged at alternating angles of 45° , and its supplementary angle.

In slender containers, the crystallization starts at the front and back walls and propagates inward (detailed description in Section 4.1). Regular structures exist almost in the entire packing volume.

For the polydisperse particle assembly, Fig. 8(a) and 8(b) show the first wall layer sphere distributions on the front wall. Large zones with regular sphere patterns are not observed, only small clusters of similar diameter particles exhibit regularities. Similar results are obtained for the side wall-4 (see Fig. 9). In both figures, the agreement between simulations and experiment is good.

3.3. Coordination number distribution

The coordination number (CN) of a particle is defined as the number of neighboring particles in contact. For mono-sized particle packing, the simulation results of coordination number distribution for the total volume and first, third and fifth layers in 'Isc' are in good agreement with the experiments, as seen from Fig. 10(a) and 10(b). The peak of CND for the third and fifth layers is at 12, and for the first layer, it is at 9, similar to the experimental findings. The maximum number of particles has a CN of 12, indicating that the obtained packing structure is close to the hexagonal close-packed structures.

For polydisperse packing, Fig. 11(a) shows the coordination number distribution for spheres in the bulk volume (the effects from all walls

were cut off). The trend obtained from the simulation is in line with the experiment. The peak is observed at 7, equal to the mean value for the bulk zone in random close packing as described in [64]. The coordination number of spheres in the bulk volume with respect to their diameter is shown in Fig. 11(b). The coordination increases with the increase in diameter in accordance with the experimental observation [64].

3.4. Voronoi packing fraction

Voronoi packing fraction for the particles shows the extent of closed packing in the assembly by analyzing the geometrical arrangement of the particles. For the mono-sized assembly, the probability distribution of the Voronoi packing fraction is calculated for mid-layers, 4th, 5th and 6th layers along x-direction and compared with 5th layer of experiments. The VPFD has a peak at 0.74 in the wall layers, characteristic for a dense closed packing structure, see Fig. 12(a). Another peak is also noticed at 0.68; it is due to a few clusters of spheres formed because of internal disturbances. For the polydisperse assembly, Fig. 12(b), the Voronoi packing fraction has a maximum at about 0.64 in the bulk volume, characteristic for random close packing. The simulation curve is slightly shifted to higher values than the experiments because of the larger packing fraction obtained by simulation, compare Section 3.1.

In Section 3, with experiments, an impressive agreement of the DEM simulations with the experimental results is shown. In Sections 4 and 5, results from further DEM simulations are reported to describe the mechanism of filling and the effect of varying system properties on the final packing structure.

4. Effect of vibration on mono-sized particle packing

In this section, the influence of vibration on the mono-sized particle packing is analyzed. Here the packing structures of the mono-sized assemblies with and without vibration (gravity filling) (cases SM1 and SM2* in Table 2) are investigated. In gravity filling, the particles are filled continuously without vibration into the inclined container. After complete filling, the container is rotated back to a horizontal position. The VFD, CND, and VPFD were analyzed for the packing with and without vibration, as shown in Fig. 13(a) to 13(c) respectively. The high void fractions, lower peaks of coordination number, and Voronoi packing

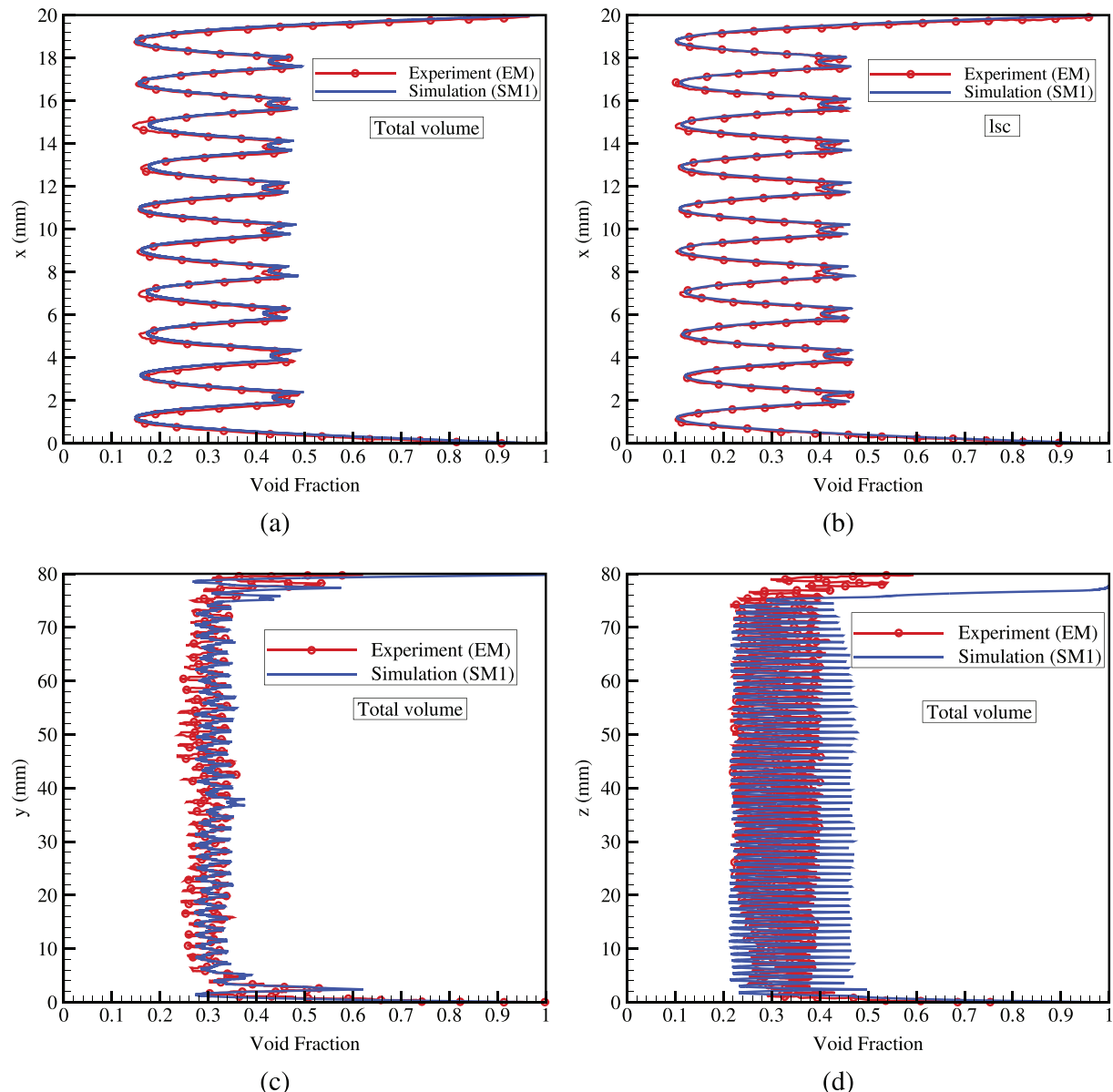


Fig. 3. Comparison of void fraction distribution obtained in simulations with experiments [64] along (a) x-direction, (b) x-direction for large slender container (lsc), (c) y-direction, and (d) z-direction for mono-sized particle assembly. [Color online].

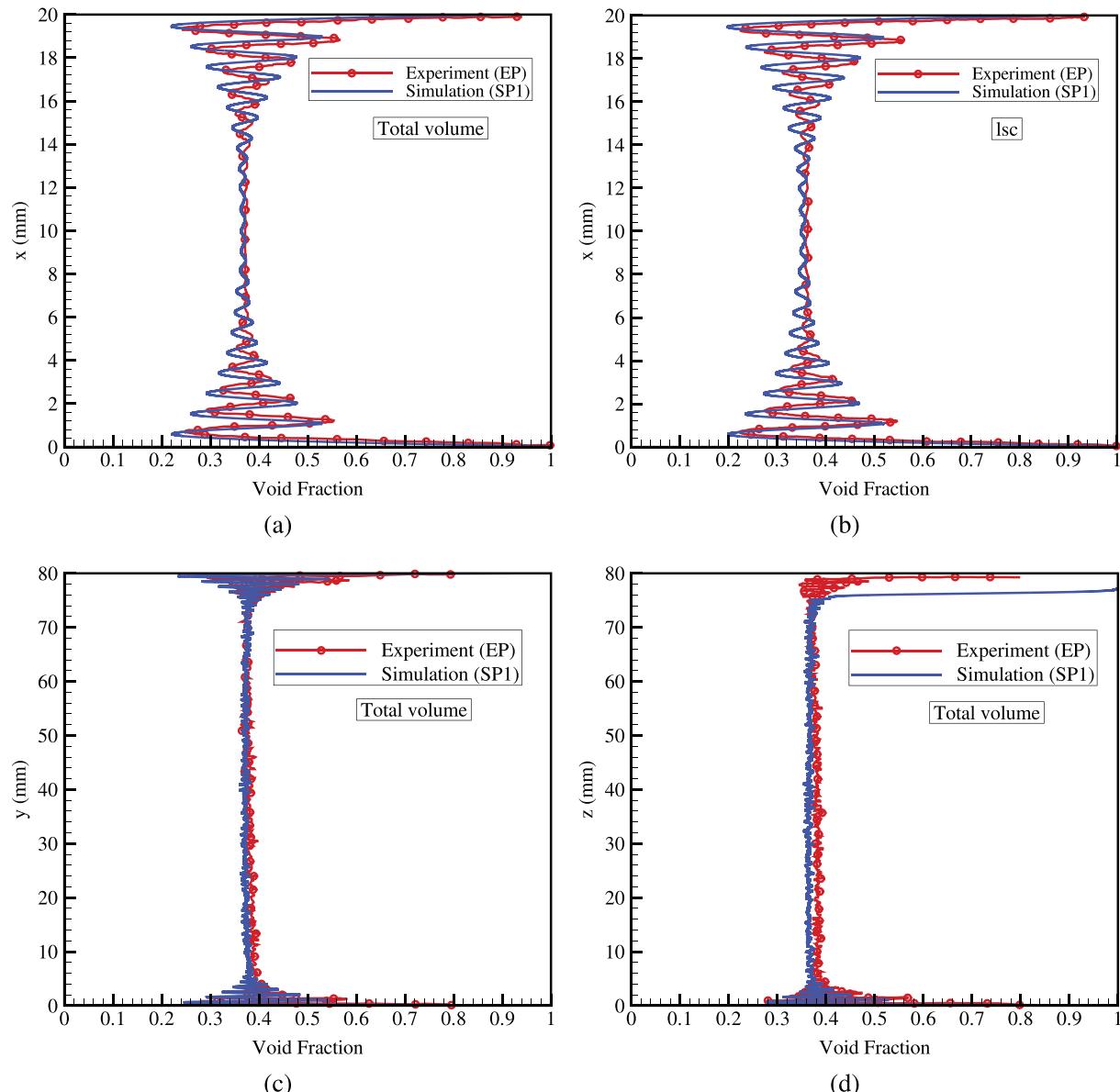


Fig. 4. Comparison of void fraction distribution for polydisperse particle assembly obtained in simulations with experiments [64] along (a) x-direction, (b) x-direction for large slender container (lsc), (c) y-direction, and (d) z-direction. [Color online].

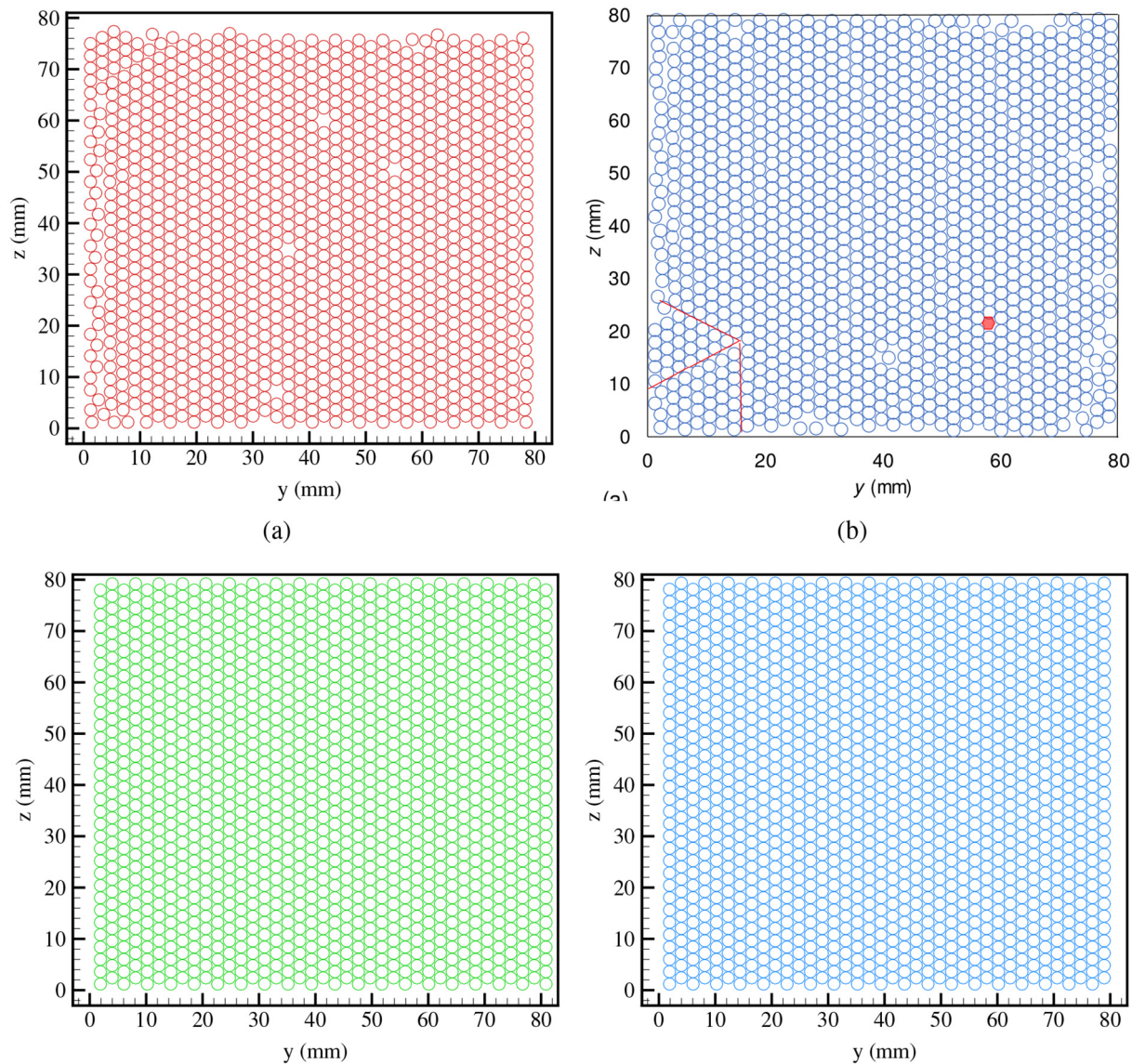


Fig. 5. Visualization of first wall layer of front wall for (a) simulations (SM1), (b) experiment (EM) [64], and ideal cases: (c) ABAB stacking and (d) ABCABC stacking. [Color online].

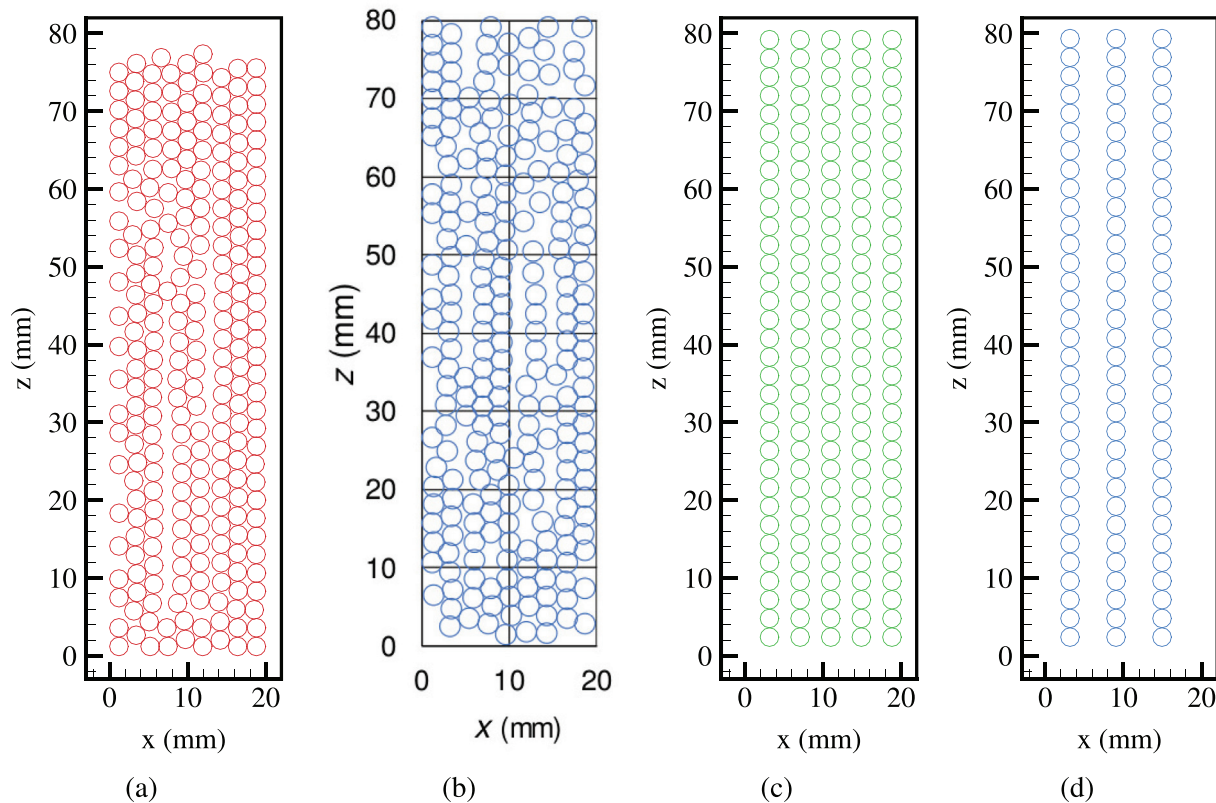


Fig. 6. The distribution of first wall layer spheres on side wall-4 for (a) simulations (SM1), (b) experiment (EM) [64], and ideal cases: (c) ABAB model and (d) ABCABC model. [Color online].

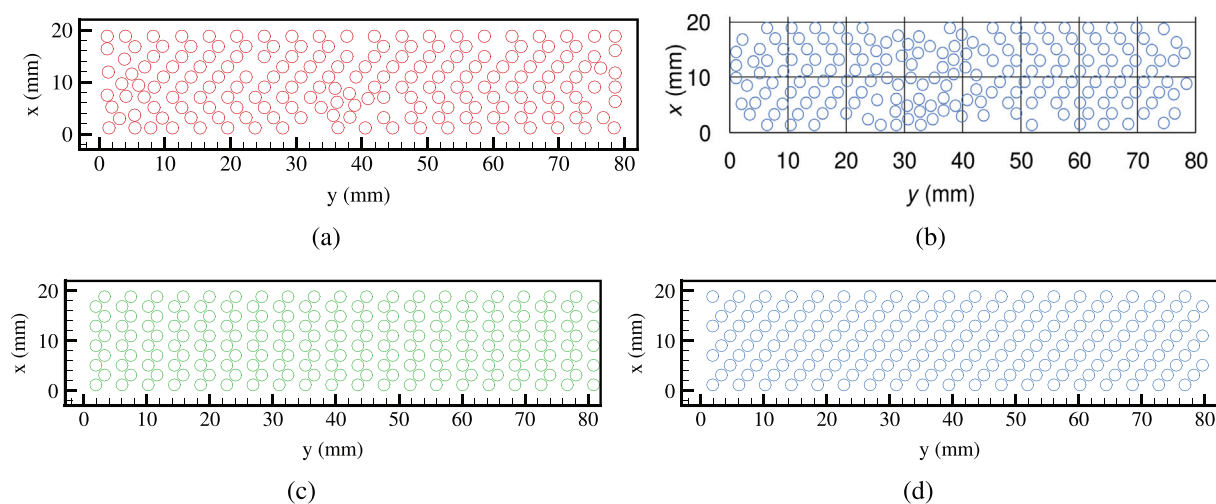


Fig. 7. Sphere distribution on first wall layer of side wall-3 for (a) simulations (SM1), (b) experiment (EM) [64], and ideal cases: (c) ABAB model and (d) ABCABC model. [Color online].

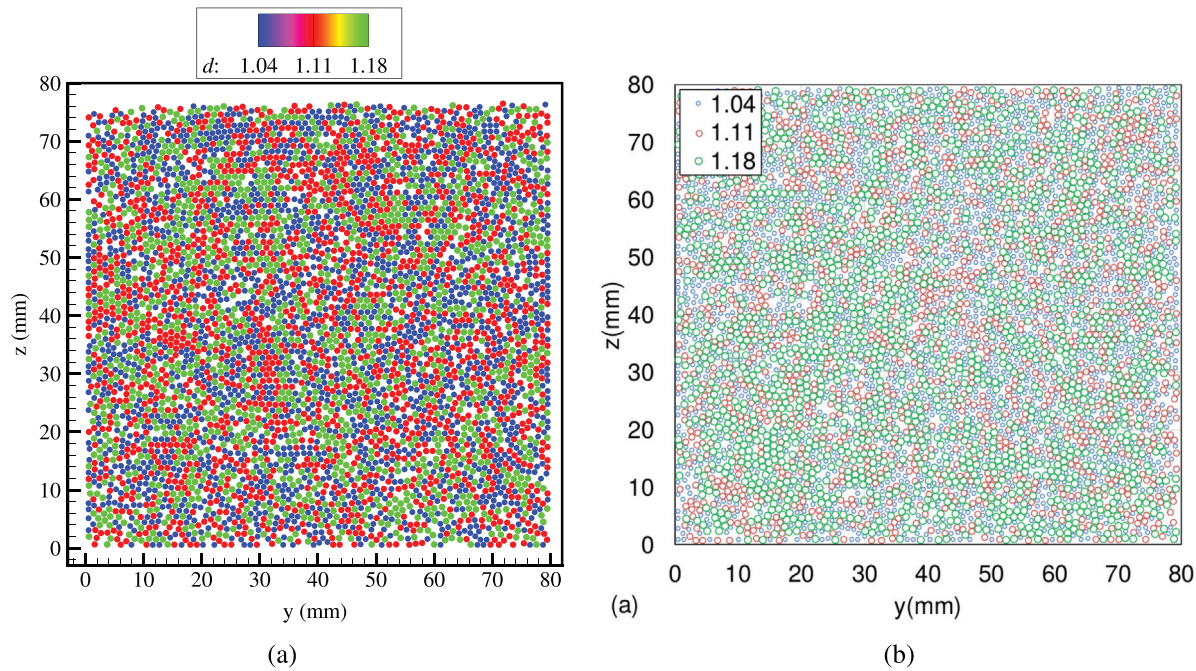


Fig. 8. Sphere distribution on first wall layer of front wall for (a) simulations (SP1) and (b) experiments (EP) [64] for polydisperse particle assembly. [Color online].

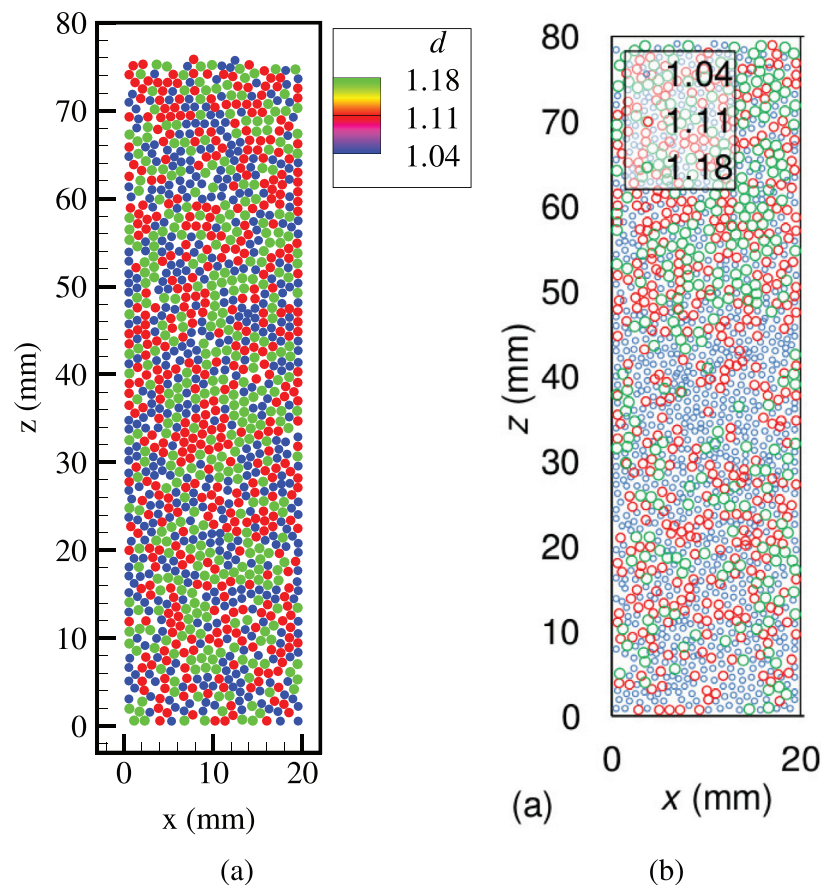


Fig. 9. Sphere distribution on first wall layer of side wall-4 for (a) simulations (SP1) and (b) experiments (EM) [64] for polydisperse particle assembly. [Color online].

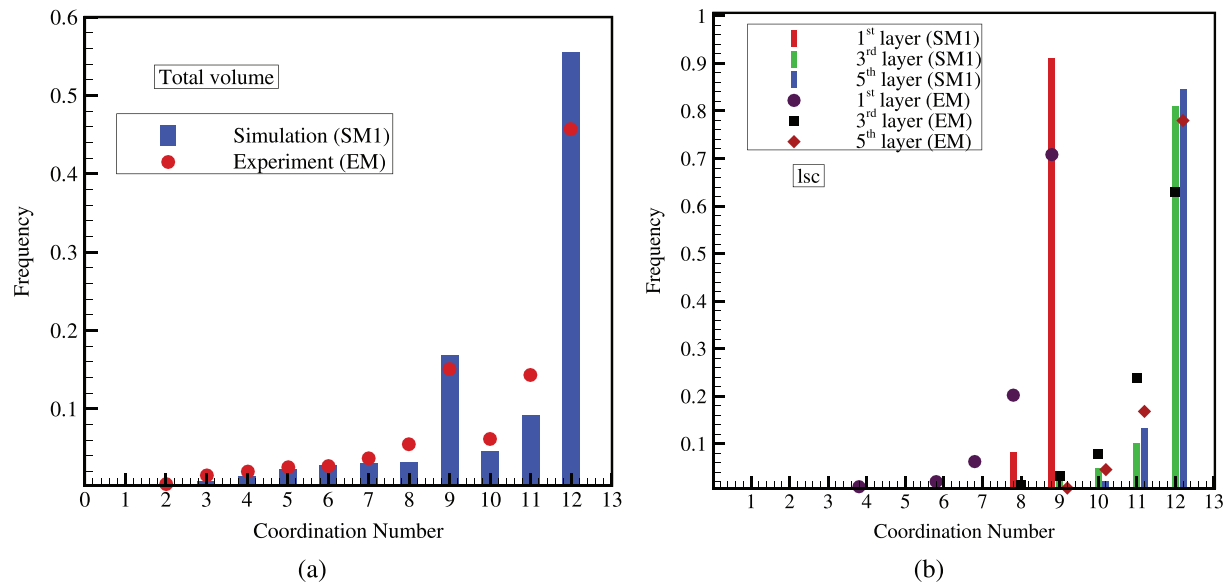


Fig. 10. Coordination Number distribution for mono-sized assembly in (a) Total volume, (b) different wall layers in 'lsc'. [Color online].

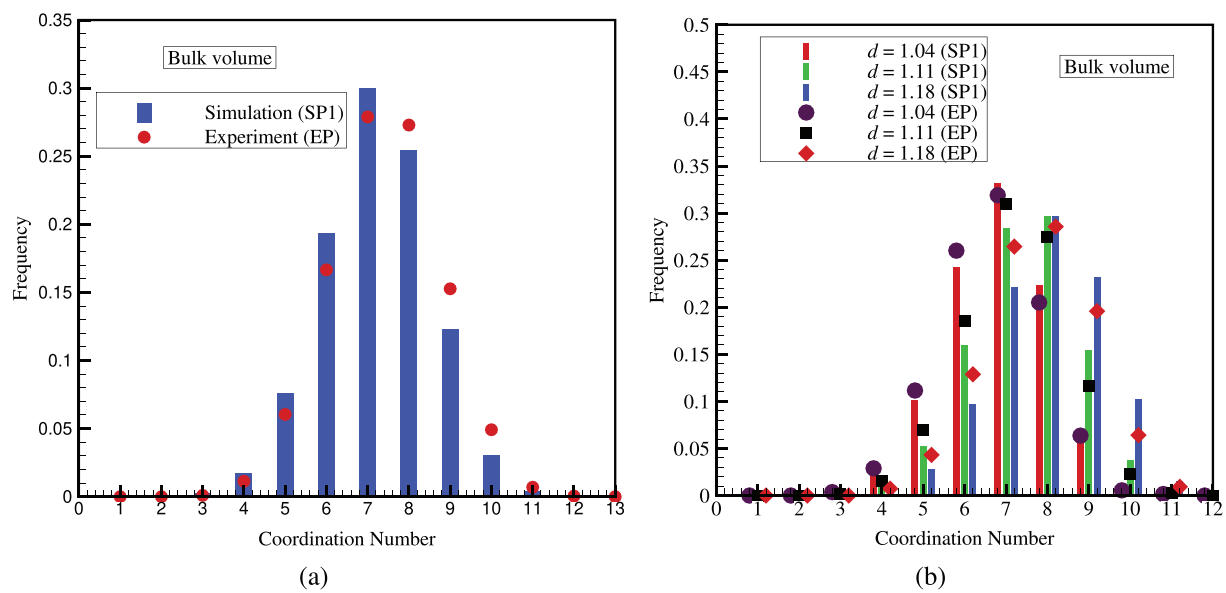


Fig. 11. Coordination number distribution for polydisperse particle packing for (a) bulk volume, and (b) different diameter groups in bulk volume. [Color online].

fraction depict that loose packing with high randomness exists in the packing without vibration. It may be noted that the packing fraction of total volume, without vibration ($\gamma_{\text{total}} = 0.5935$), is much less compared to the packing structure obtained with vibration ($\gamma_{\text{total}} = 0.675$) as listed in Table 2. A similar comparison is carried out by Desu et al. [24] but with different particle and vibration parameters for cubical containers. The evolution of packing structure with vibration is described in Section 4.1. It may be noted that for the experimental validation shown in Section 3, the volumes used for the calculation of VFD, CND, VPFD were different for different mean diameters. However, in Sections 4 and 5, the volumes were calculated consistently with respect to mean diameter as listed in Table 5.

4.1. Transient response of the mono-sized particle assembly

In this section, the evolution of the packing structure during the vibration-assisted filling is investigated for the mono-sized particles. The overall packing fraction and the void fraction distribution are analyzed at regular intervals during the vibration period between consecutive filling steps. Fig. 14 shows the overall packing fraction of the assemblies during steps of filling with the duration of vibration (15 s). The 60% filled indicates the first filling step; the inclined container is filled up to 60% volume and followed by vibration (for 15 s). After the vibration, the container is filled to 80% volume and vibrated for 15 s, and this is the second step of filling, represented as 80% filled. Similarly, 92% filled is the third step of filling, and in the fourth filling step, the inclined container is filled up to 94% volume and rotated to the horizontal position and vibrated for 15 s. For 60% filled container vibration (first vibration stage), packing fraction is seen to increase significantly with vibration time. Vibration promotes the spheres to occupy a stable configuration, settling in a regular close-packed arrangement, thereby increasing the packing fraction of the assembly. For the subsequent filling steps, the resulting structure from step one serves as a template, and the increase of overall packing fraction is moderate.

Fig. 15 shows void fraction distribution for 'lsc' volume along x-direction, at different time intervals (t). For the 60% filled stage (as mentioned above) (Fig. 15(a)), the particles become regularly arranged with increasing time. From about 9 s onward, every wave has double-peaked maxima, a characteristic of the dense hexagonal packing. It is also observed that waves with double-peaked maxima are formed at the walls and progressed later into the bulk, indicating the start of crystallization at the walls.

Similar to the findings for overall packing fraction, with subsequent vibration stages (second, third and fourth filling), the VFD patterns do not change much except for a slight shift towards lower porosities, (see Fig. 15(b) to 15(d)). As the transient response of the packing structure is analyzed, the effect of vibration amplitude and frequency on the packing structure is explained in the following section.

4.2. Effect of the vibration amplitude and frequency on the packing structure

In this section, parametric analysis of vibration amplitude and frequency on the packing structure is studied. A similar filling procedure was followed as explained in Section 2 with the change in vibration parameters. The list of cases carried out along with the total and 'lsc' packing fraction are tabulated in Table 3. The Fig. 16(a) and 16(b) show the packing fraction with different frequencies of vibration for total volume and 'lsc' volume, respectively. For the amplitude considered, the packing fraction for both total volume and 'lsc' volume increases with an increase in frequency to a maximum and decreases. Similar findings are reported for mono-sized packing with 3D vibration by An et al. [55]. As the energy input increases, particle rearrangement eliminates voids in the initial packing, thereby increasing packing density. However, with too high energy, the particles get highly excited, leading to disturbance in order structure, resulting in lower packing density.

The Fig. 17(a) to 17(d) show the void fraction distribution along x-direction for 'lsc' volume for amplitudes $a = 0.2, 0.3, 0.6, 1.2$ mm, respectively. Similar conclusions as discussed above can be drawn from

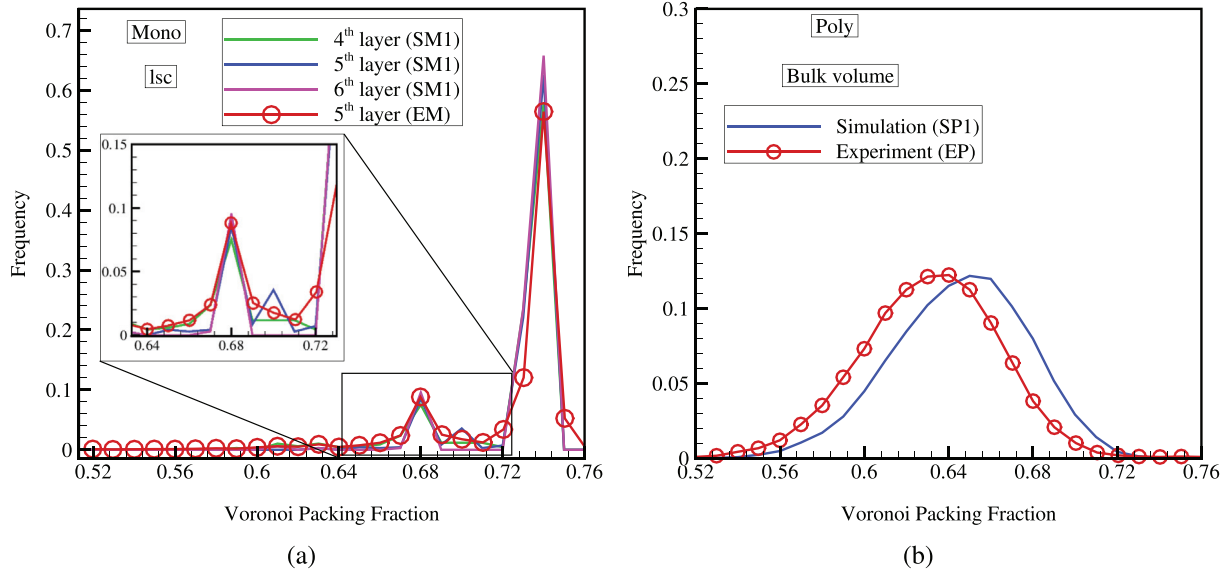


Fig. 12. Voronoi packing fraction of (a) mono-sized particle assembly, (b) poly disperse particle assembly. [Color online].

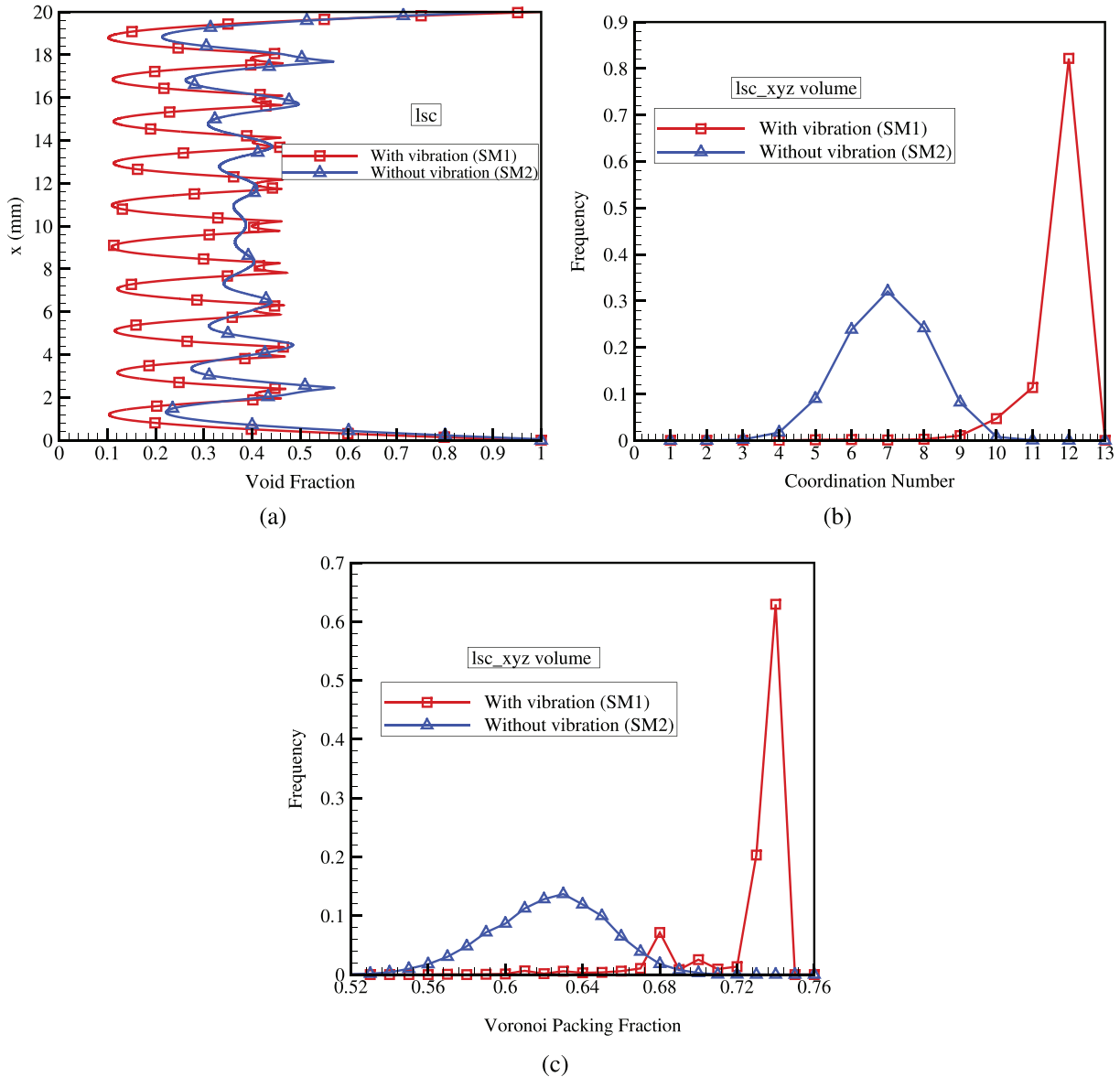


Fig. 13. Comparing packing structure with and without vibration (a) Void fraction distribution in x-direction, (b) Coordination number distribution, (c) Voronoi packing fraction distribution. [Color online].

the void fraction distributions. For a considered amplitude, the minima of void fraction distributions decreases signifying an increase in packing fraction (see Fig. 17(a) to 17(d)). The variation of void fraction with increase in frequency of vibration is larger for smaller amplitudes (Fig. 17(a) and 17(b)) compared to larger amplitudes (Fig. 17(c) and 17(d)). Based on this analysis, the amplitude and frequency of vibration are chosen to be 0.6 mm and 100 Hz, respectively, for all other simulations.

4.3. Effect of orientation of the container and direction of vibration

The influence of container orientation on the packing structure during the filling process is analyzed, considering a horizontal container

and an inclined container (45° orientation). The schematic of the container in horizontal and inclined orientations is shown in Fig. 2(a) and 2(b), respectively. The filling procedure and vibration parameters are maintained to be the same for comparing the resulting packing structure. The VFD along x, y, and z directions for both the cases are shown in Fig. 18(a) to 18(d), respectively. It is observed that a slight disturbance in sphere distribution i.e., a boundary formed between two stable configurations in the y-direction is reflected in reduction of local VFD, as seen in Fig. 18(c). As the container is slender, this kind of pattern is present in all sphere layers from wall to the wall in the shortest width direction (x-direction). However, the VFDs along x and z directions, CND and VPFD are almost similar for both the cases, as shown in Figs. 18(a), 18(b), 18(d), 19(a) and 19(b), respectively. And also, the difference in

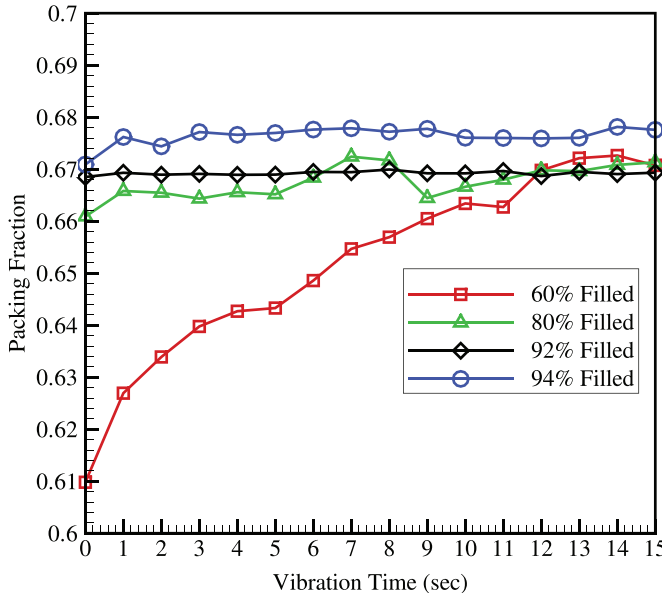


Fig. 14. Evolution of overall packing fraction with vibration time for mono-sized particle assembly. [Color online].

the overall packing fraction for both horizontal and inclined containers is observed to be only 0.69%. Thereby, the resulting packing structure is observed to be independent of the container orientation, similar to the experimental observations [64]. Inclined containers are most beneficial only in the applications that require complete filling of containers; as seen from Fig. 18(d), the particles occupy greater height in the inclined container than the horizontal container.

The influence of vertical and horizontal vibration on the packing structure is analyzed for both inclined and horizontal containers. The horizontal container is vibrated along with the container's x, y, and z-axis (global coordinates of the container), as shown in Fig. 2(a). On the other hand, the inclined container is vibrated along x', y' and z' direction (not global coordinates of the container). The direction of vibration of the inclined container is similar to the horizontal container as shown in Fig. 2(b). Fig. 20 shows the VFD, CND, VPFD for both the orientations in different directions. The packing structure with vibration in the x-direction is poor with high average void fractions and lower peaks of CND and VPFD, as the slender dimension does not provide enough space for the particle rearrangements. The plots depict that assemblies obtained by vibration in the y-direction are better than the vibration in the x-direction but not denser than the vibration in the z-direction. Vertical vibration in both orientations results in dense packing structure compared to horizontal vibration, which may be attributed to the influence of gravity and space availability.

5. Factors influencing polydisperse packing

The packing structure obtained for polydisperse particle packing is different from mono-sized particle packing, as described in Section 3.1. The factors that influence polydisperse packing are:

1. Ratio of the container's dimension to the mean particle diameter (X/d_m ratio).
2. Polydispersity ($\lambda = (r_{\max} - r_{\min})/d_m$) of particle size distribution.

5.1. The influence of mean particle radius on polydisperse packing

To understand the influence of mean particle diameter on the packing structure, a non dimensional parameter X/d_m is considered, where d_m is the mean diameter of the particles and X is the distance between parallel walls of the container in x-direction. The polydisperse packing cases SP2, SP3, SP4 with $X/d_m = 12.5, 9.01$, and 8.33 as listed in Table 2 were analyzed and compared along with previous simulated mono-sized (case SM1 with $X/d_m = 8.33$) and polydisperse particle packing (case SP1 with $X/d_m = 18.01$).

The filling strategy followed for the above cases was similar to previous simulations, as discussed in Section 2. The VFDs along the x-direction in 'lsc' volume are shown in Fig. 21(a) to 21(e), it is observed that with decrease in X/d_m , the bulk volume decreases as only few layers are formed and resulting in slightly lower packing fraction as reported in Table 2, similar findings are reported for pebble packing in cylindrical containers [60]. For polydisperse case SP4 with $X/d_m = 8.33$, only a total of 10 layers are formed, resulting in the interlocking of wall effect from opposite walls showing the influence in the entire volume. However, in the case SP1, many layers are formed as X/d_m is higher, and the influence of the wall is seen only up to 4–5 layers as reported by Reimann et al. [48], thereby leading to the formation of bulk volume. The resulting packing structure for polydisperse packing (with the same polydispersity) is observed to be depend on X/d_m . However, the X/d_m ratio has no significant effect on the contact number (Fig. 22(a)) and Voronoi packing fraction distributions (Fig. 22(b)).

The mono-sized case and polydisperse case SP4 have the same value of X/d_m and polydispersity equal to 0 and 0.063, respectively. For the polydisperse case SP4, even though the wall effect is observed in the entire volume, the assembly has not attained dense packing similar to mono-sized assembly (absence of double-peaked maxima). This is due to particle size distribution, i.e., the regular arrangement is disturbed due to particles of different sizes (discussed in Section 5.2). Therefore, the resulting packing fraction obtained is much less than the mono-sized packing with the same X/d_m .

5.2. Effect of polydispersity on the polydisperse packing

The variation in the particle diameters in a polydisperse assembly is quantified using polydispersity, defined as $\lambda = (r_{\max} - r_{\min})/d_m$. The influence of λ on the packing structure is analyzed using the polydisperse cases SP9, SP11, SP13, SP15 with $\lambda = 0.0021, 0.0063, 0.021, 0.063$ as listed in Table 2.

Fig. 23(a) and 23(b) show VFD along x-direction of polydisperse assemblies with varying polydispersity. With the decrease in polydispersity, the assembly is approaching closer to dense packing as the orderliness of the structure increases from the wall, leading to a decrease in the bulk volume, even though X/d_m is the same for all the cases. Within the range of λ considered, packing fraction increases with a decrease in polydispersity as listed in Table 2. The peaks of CND and VPFD (see Fig. 23(c) and 23(d)) were shifted to higher values signifying the increase in the orderliness of the assembly with a decrease in λ value.

A few more polydisperse packing cases with much lower λ values are considered as listed in Table 2, and the packing structure is similar to $\lambda = 0.0021$. The packing structure with $\lambda = 0.0021$ and $X/d_m = 8.33$ is very similar to the mono-sized packing. Thus, there seems to be a transition from mono-sized packing to polydisperse packing with varying values of λ , which is discussed in Section 5.3.

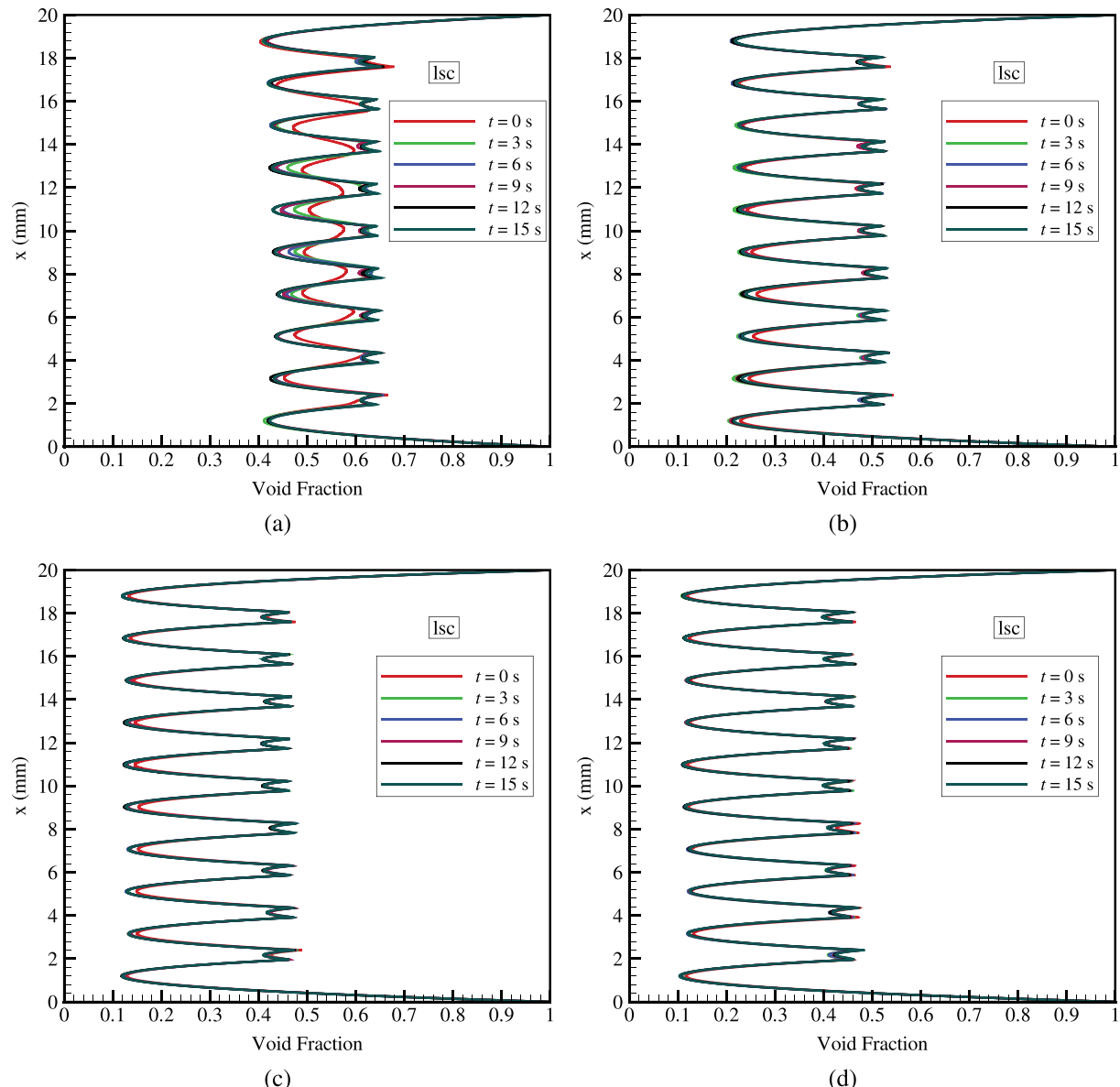


Fig. 15. Transient response of mono-sized assembly for (a) 60%, (b) 80%, (c) 92%, (d) 94% filled containers. [Color online].

Table 3
Parametric analysis of amplitude and frequency of vibration.

	Cases	Amplitude, a (mm)	Frequency, f (Hz)	γ_{total}	γ_{isc}
Mono-sized $d_m = 2.4$ mm DEM Simulations	SV1	0.2 (or) 0.0833^*d_m	25	0.614	0.632
	SV2		50	0.656	0.684
	SV3		75	0.647	0.681
	SV4		100	0.654	0.689
	SV5		200	0.644	0.681
	SV6		400	0.649	0.680
	SV7	0.3 (or) 0.125^*d_m	25	0.629	0.656
	SV8		50	0.656	0.688
	SV9		75	0.650	0.688
	SV10		100	0.660	0.698
	SV11		200	0.650	0.690
	SV12		400	0.650	0.681
	SV13	0.6 (or) 0.25^*d_m	25	0.665	0.696
	SV14		50	0.662	0.699
	SV15		75	0.663	0.710
	SV16		100	0.671	0.710
	SV17		200	0.655	0.689
	SV18		400	0.656	0.687
	SV19	1.2 (or) 0.5^*d_m	25	0.671	0.710
	SV20		50	0.667	0.715
	SV21		75	0.670	0.711
	SV22		100	0.671	0.711
	SV23		200	0.665	0.710
	SV24		400	0.654	0.697

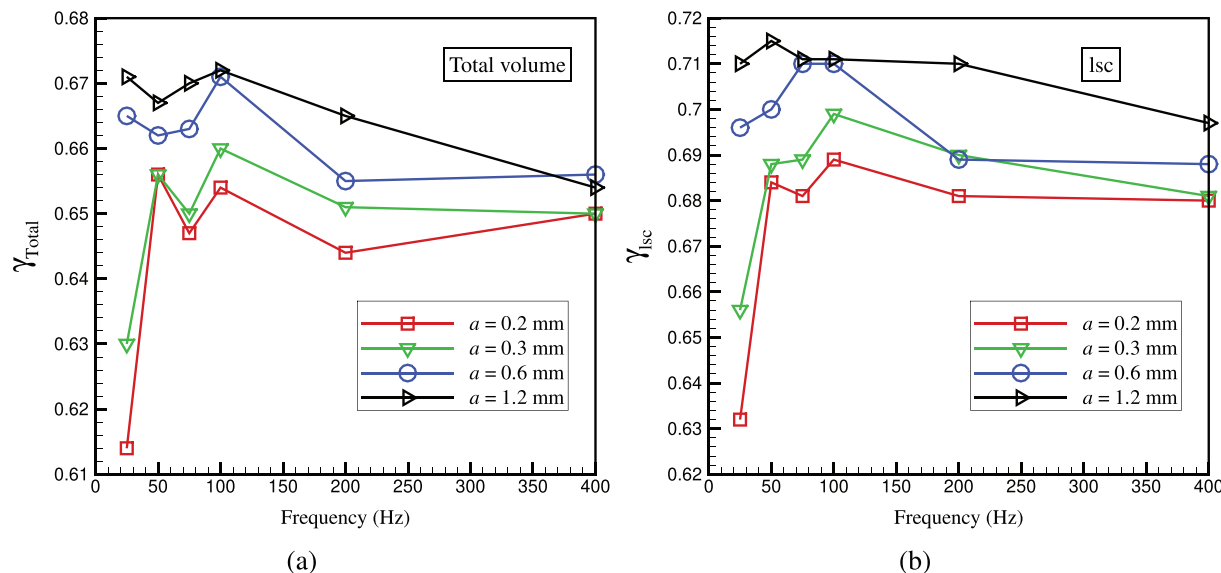


Fig. 16. The packing fraction for (a) total volume, and (b) large slender container (lsc) for various vibration frequencies. The packing fractions were calculated after 15 s of vibration. [Color online].

Table 4

Nomenclature for different volumes used for calculation of VFD, CND, VPFD.

Nomenclature	Mean diameter of the particles (d_m)	Cutoff wall thickness
large slender container (lsc)	2.4 mm 1.11 mm	10 mm at all side walls 5 mm at all side walls
Bulk volume	1.11 mm	5 mm at all walls

Table 5

Nomenclature for different volumes used for calculation of VFD, CND, VPFD.

Nomenclature	Mean diameter of the particles (d_m)	Cutoff wall thickness
large slender container (lsc)	2.4 mm 1.11 mm	$2d_m$ wall layers are cutoff from all side walls $5d_m$ wall layers are cutoff from all side walls
lsc_xyz	2.4 mm	$2d_m$ wall layers are cutoff from all walls
Bulk volume	1.11 mm	$5d_m$ wall layers are cutoff from all walls

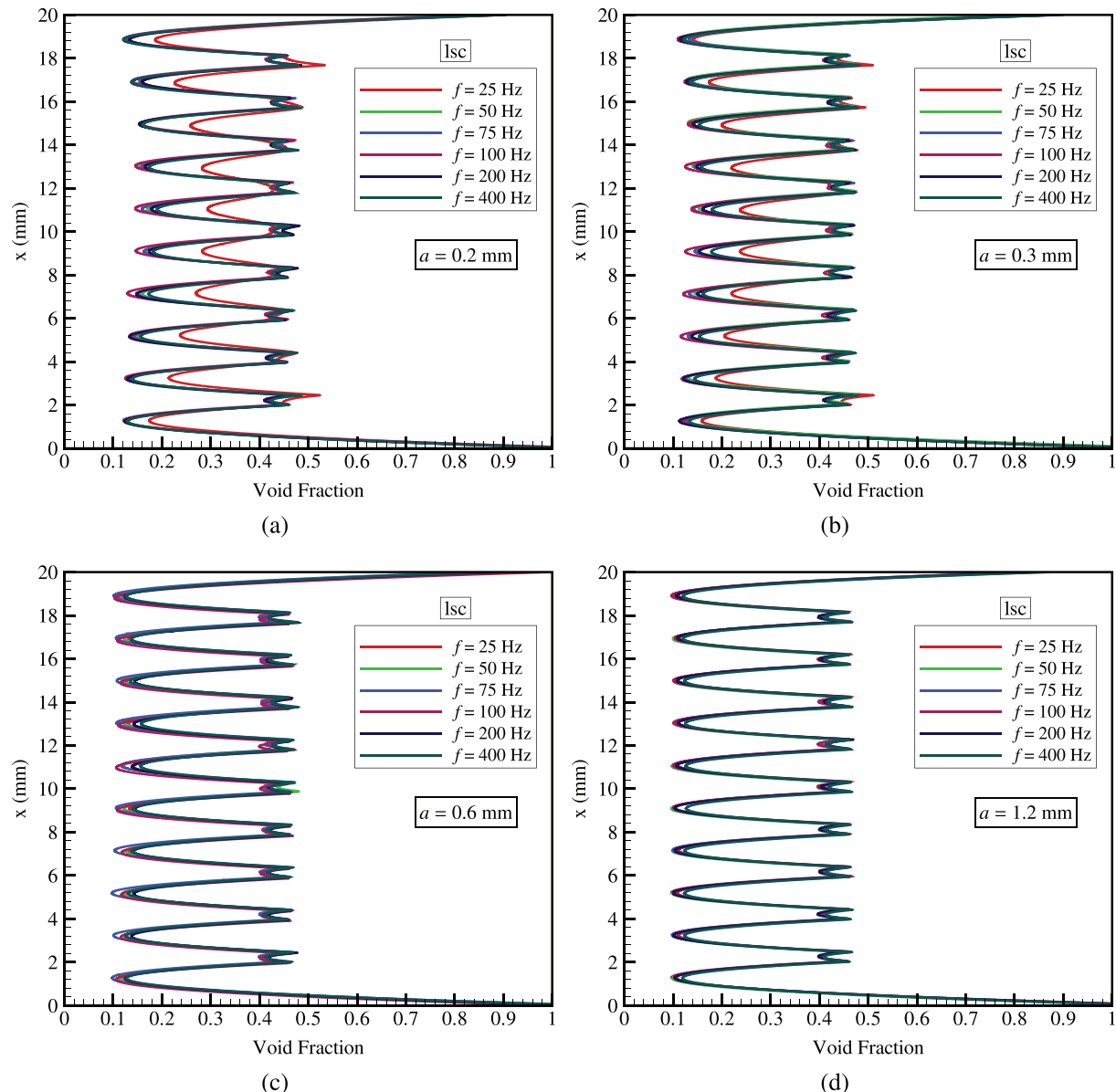


Fig. 17. Void fraction distribution (VFD) along x -direction for 'lsc' for different frequencies and with amplitude (a) 0.2 mm, (b) 0.3 mm, (c) 0.6 mm, and (d) 1.2 mm. [Color online].

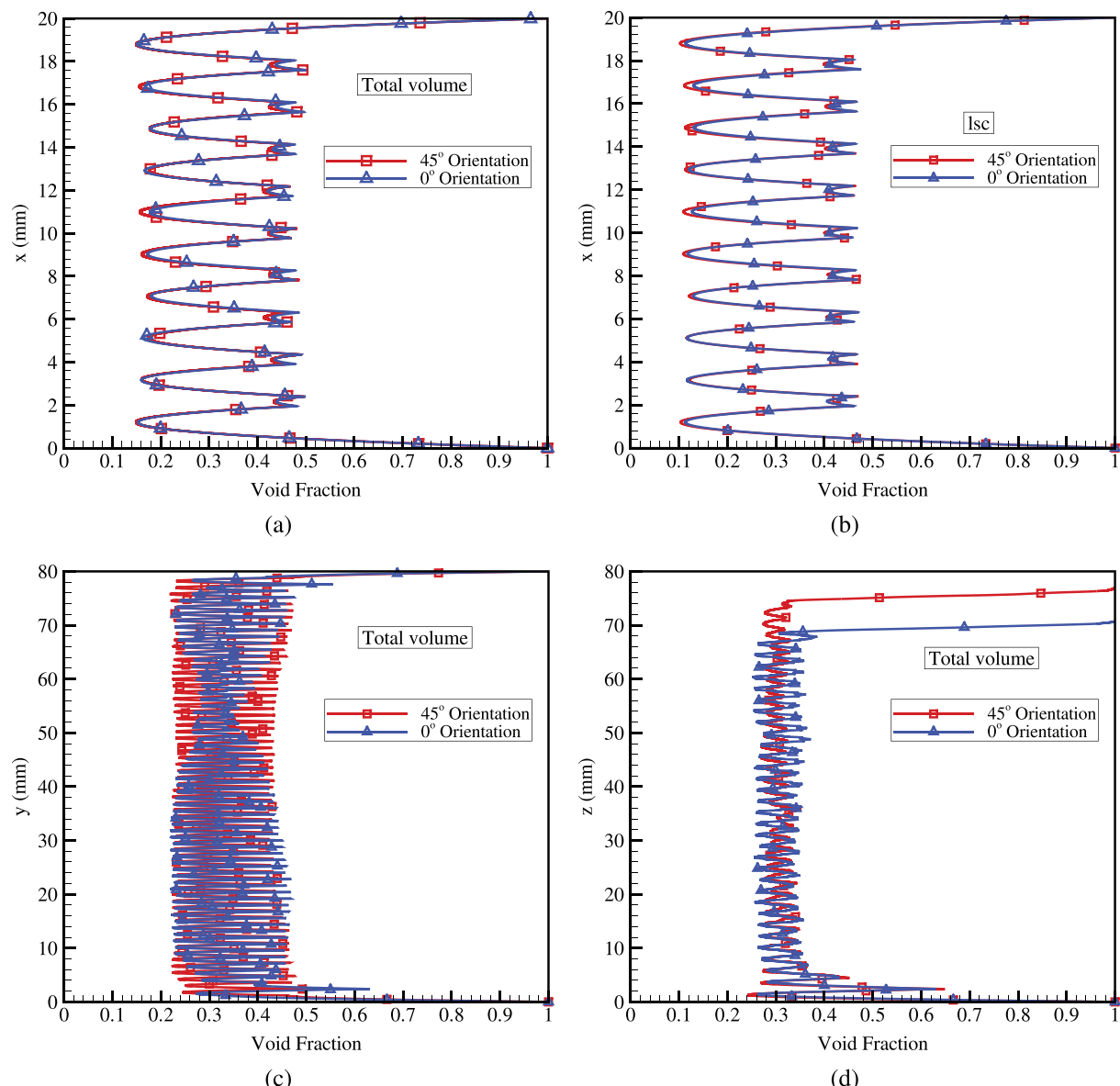


Fig. 18. Comparison of void fraction distribution along (a) x, (b) x for 'lsc', (c) y, and (d) z directions of inclined container with horizontal container. [Color online].

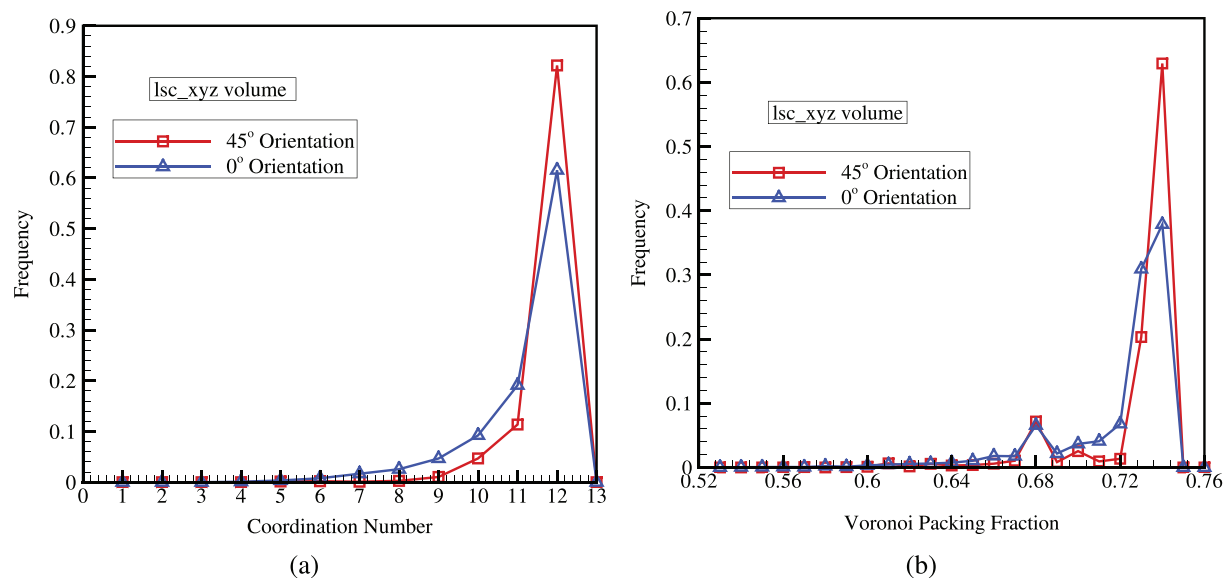


Fig. 19. Comparison of (a) coordination number distribution, (b) Voronoi packing fraction distribution of inclined container with horizontal container. [Color online].

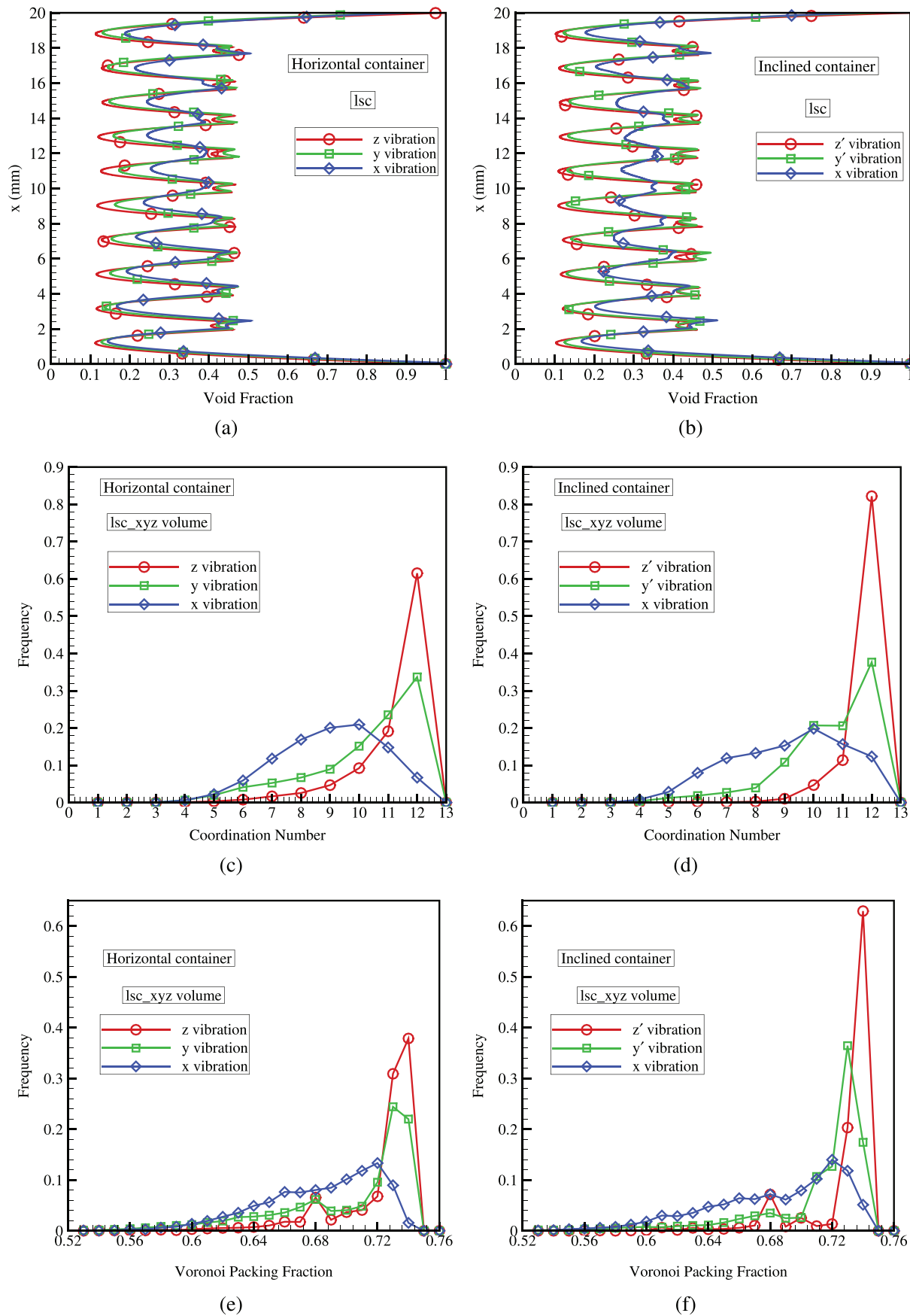


Fig. 20. Void fraction distribution along x-direction for (a) horizontal container, (b) inclined container; Coordination number distribution for (c) horizontal container, (d) inclined container; Voronoi packing fraction distribution for (e) horizontal container, (f) inclined container. [Color online].

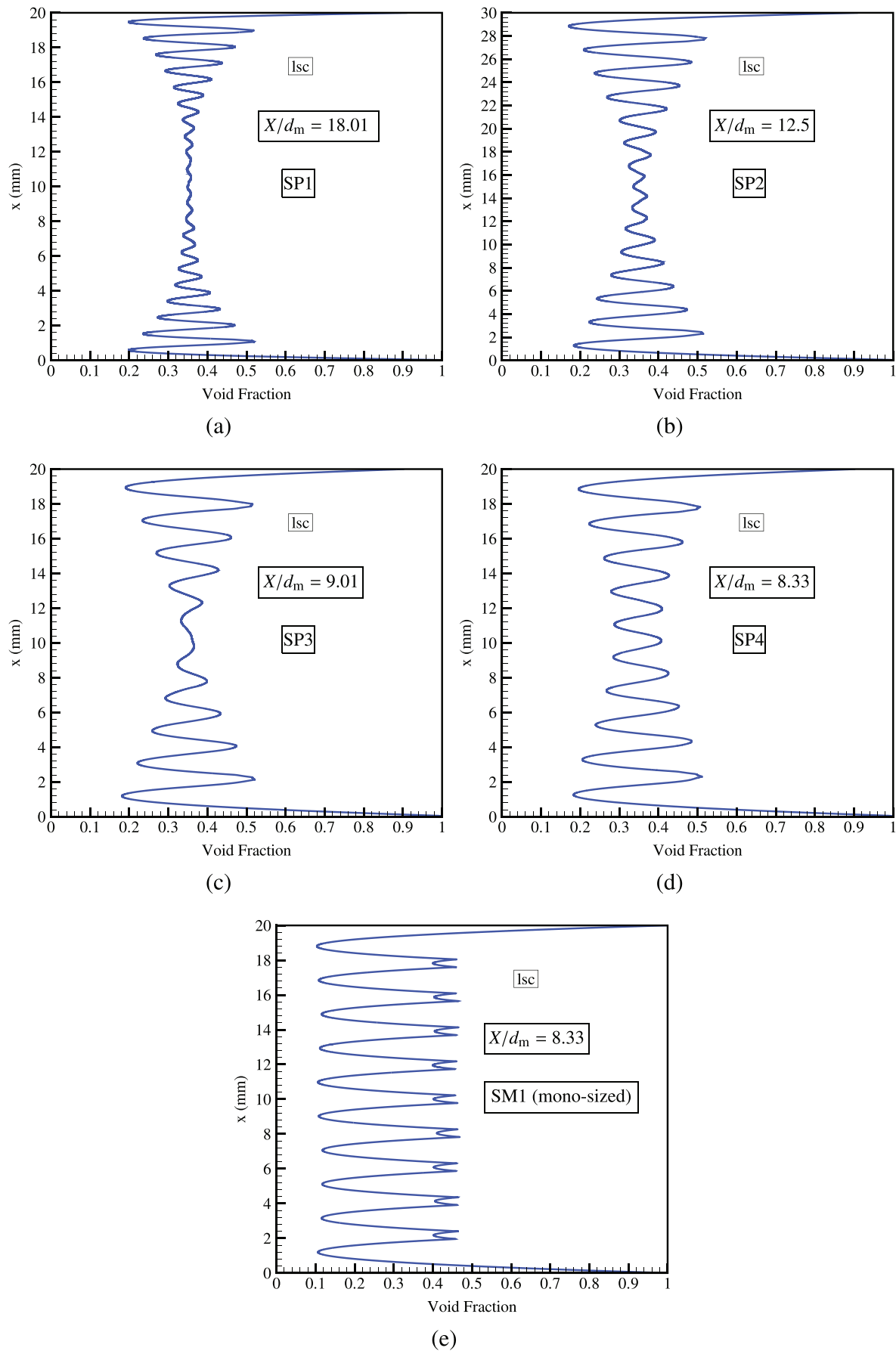


Fig. 21. Void fraction distribution along x -direction for polydisperse packing with X/d_m (a) 18.01, (b) 12.5, (c) 9.01, (d) 8.33, (e) 8.33 (mono-sized particle assembly).

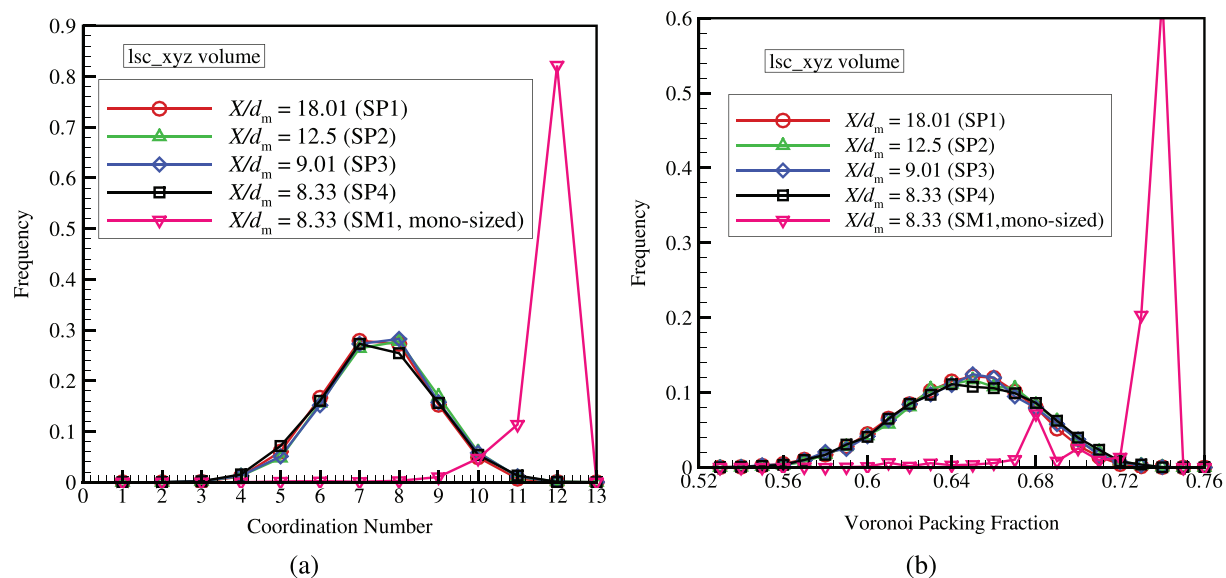


Fig. 22. Comparison of (a) coordination number distribution, (b) Voronoi packing fraction distribution for packings with different X/d_m . [Color online].

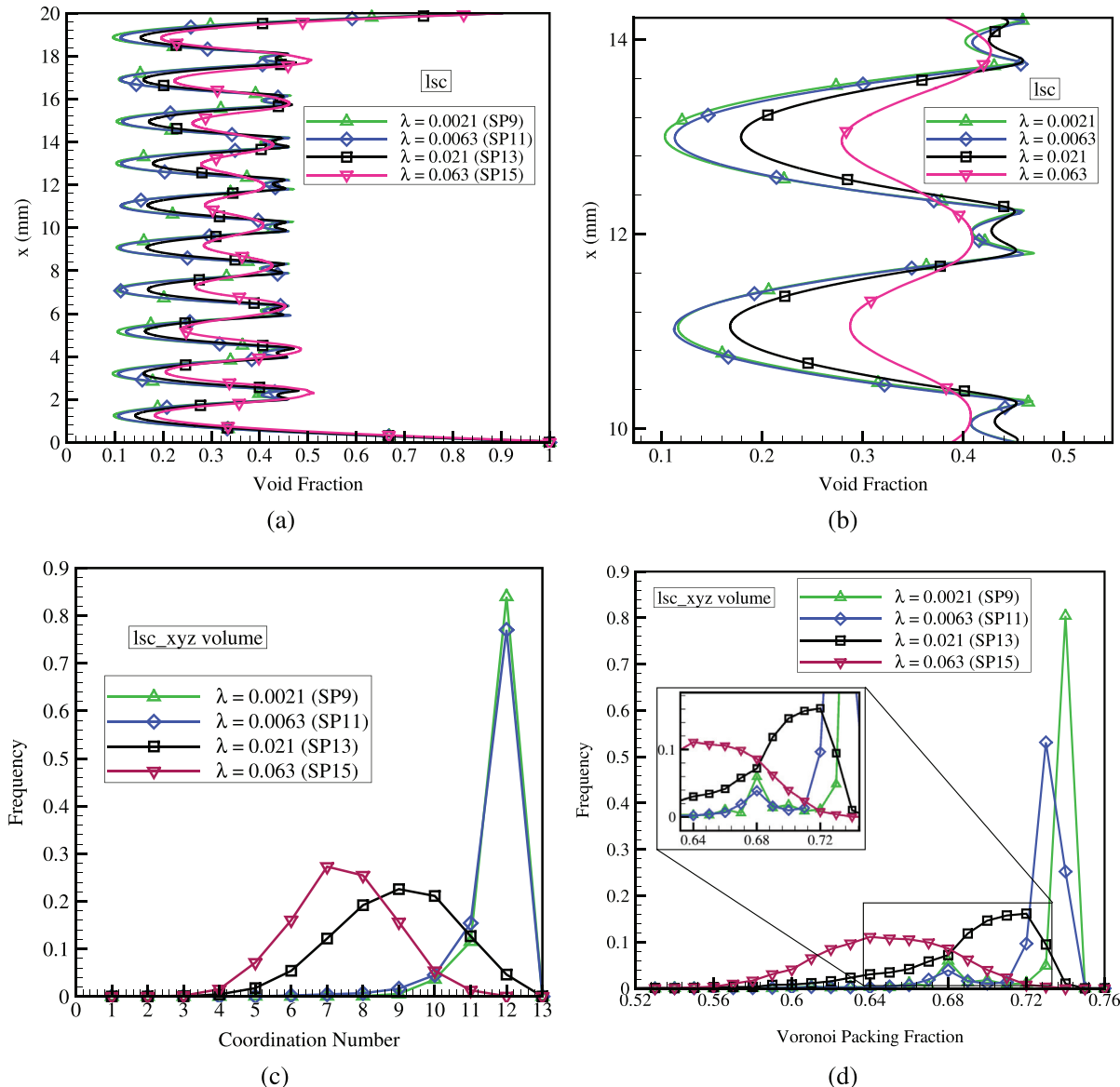


Fig. 23. Polydispersity cases with different λ (a) Void fraction distribution for 'lsc', (b) zoomed view of void fraction distribution, (c) Coordination number distribution, (d) Voronoi packing fraction distribution. [Color online].

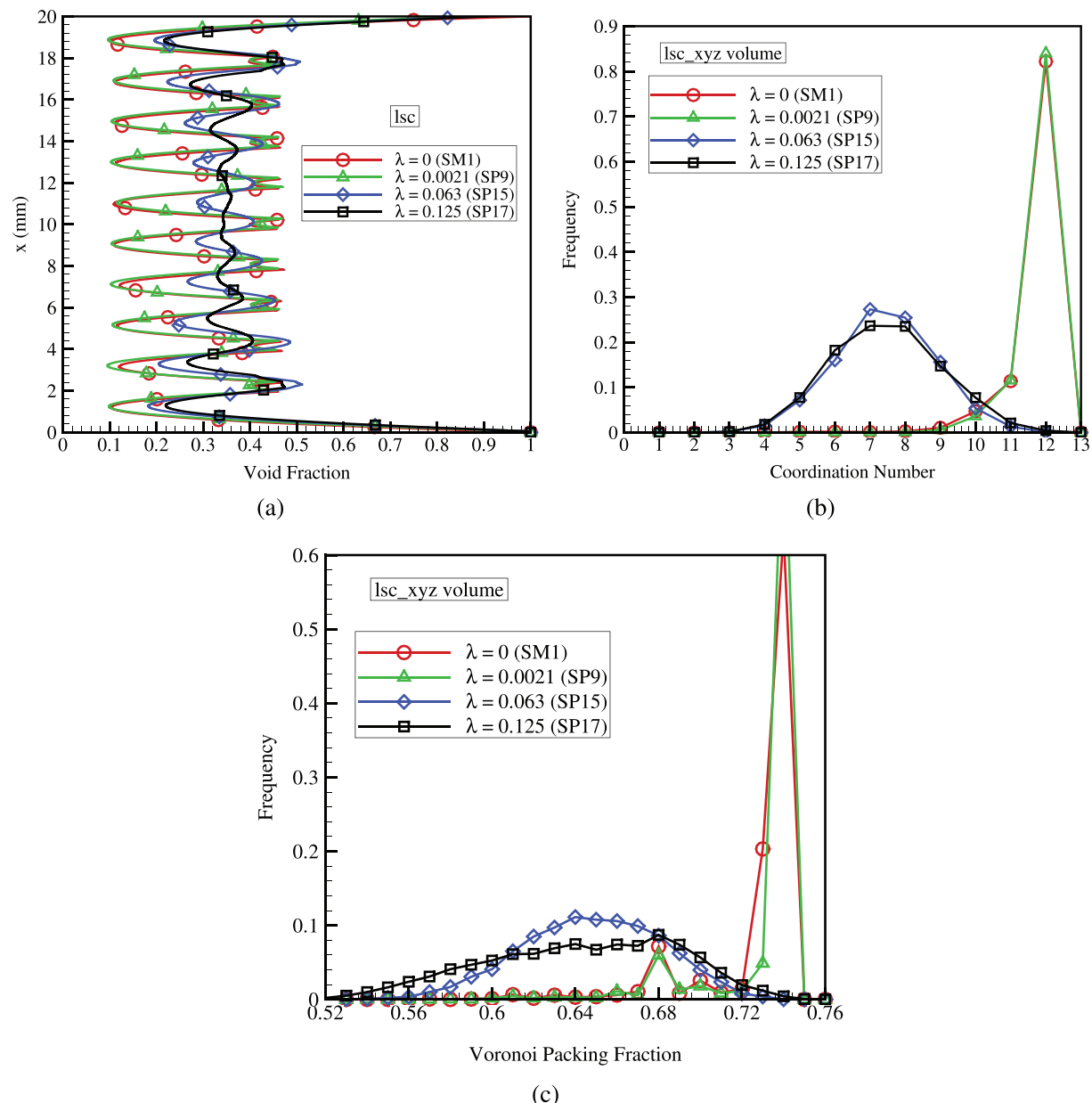


Fig. 24. (a) Void fraction distribution (VFD), (b) Coordination number distribution (CND), (c) Voronoi packing fraction distribution (VPFD) for polydisperse particle assembly with a range of polydispersity. [Color online].

5.3. Transition of packing structure from mono-sized to polydisperse packing

The polydisperse packing structure obtained with $\lambda = 0.0021$ (see Section 5.2) is similar to the mono-sized particle assembly. Here, a few more polydisperse packing are analyzed to understand the transition from mono-sized packing to polydisperse packing.

The cases like SM1, SP9, SP15, SP17 with $\lambda = 0, 0.0021, 0.063, 0.125$ as listed in Table 2 are analyzed here. The packing structure is characterized using VFD, CND, VPPD as shown in Fig. 24. The above quantities for $\lambda = 0.0021$ are in good match with mono-sized assembly, which implies that the polydisperse packing is approaching mono-sized packing. Within the range of λ studied, the packing fraction decreases with the increase in polydispersity. With the increase in λ , the orderliness decreases from the wall, and irregular arrangements occur, leading to

the bulk volume. This can be clearly observed from particle distribution on the wall layer.

Particle arrangement in the first wall layer in xy and yz plane is shown in Figs. 25 and 26. The particle distribution of polydisperse packing with $\lambda = 0.0021$, was in good agreement with mono-sized packing, compare Fig. 25(a) with Fig. 7(a), and Fig. 26(a) with Fig. 5 (a). The figures can be compared based on the wall coverage and arrangement of the spheres on the wall. Fig. 25(a) and Fig. 7(a) have similar (low) wall coverage, and the spheres are mostly seen to arrange at an angle of 45° . Fig. 26(a) and Fig. 5(a) have dense wall coverage and regular arrangement of particles with vertical chains. The particles have a regular arrangement for the assembly with $\lambda = 0.0021$, whereas the randomness increases for $\lambda = 0.063$ and 0.125 . The randomness observed on the wall layer continues in the entire container leading to bulk volume for $\lambda = 0.125$. Therefore, the variation of particle sizes in the

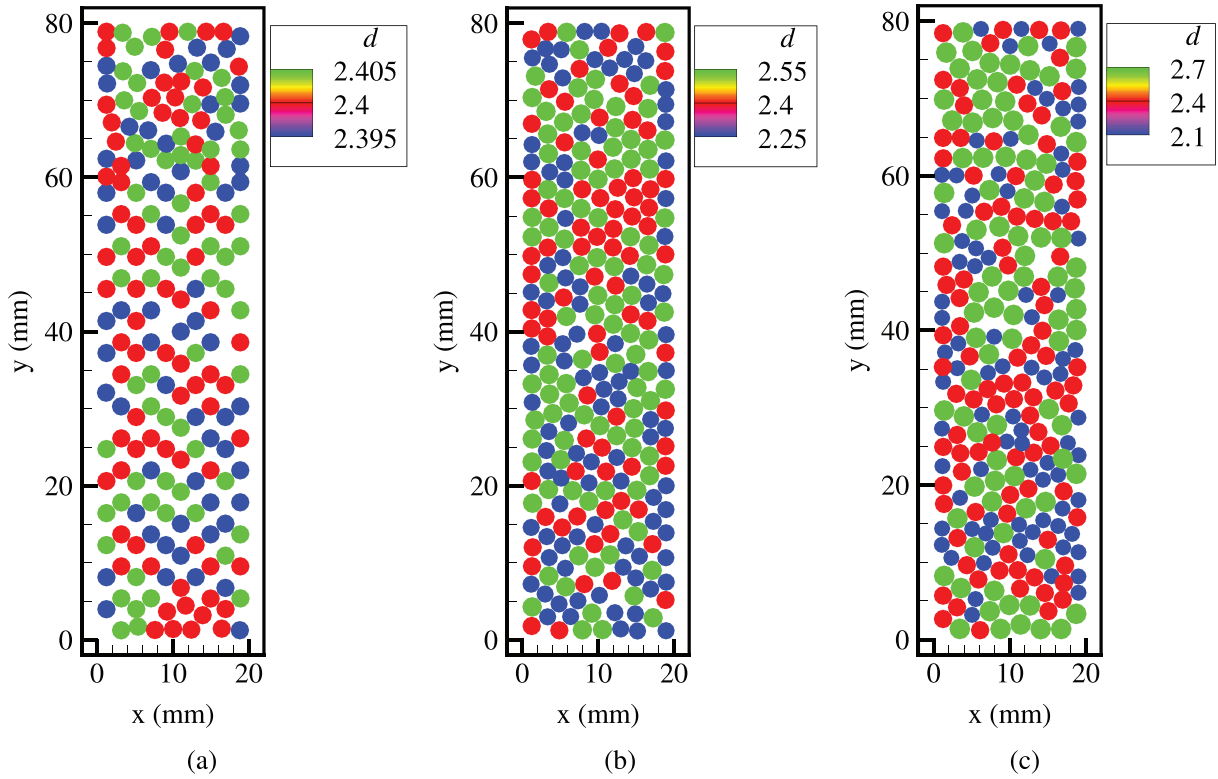


Fig. 25. The distribution of first wall layer spheres on side wall-3 for polydisperse packing with polydispersity of (a) 0.0021 (SP9), (b) 0.063 (SP15), (c) 0.125 (SP17). [Color online].

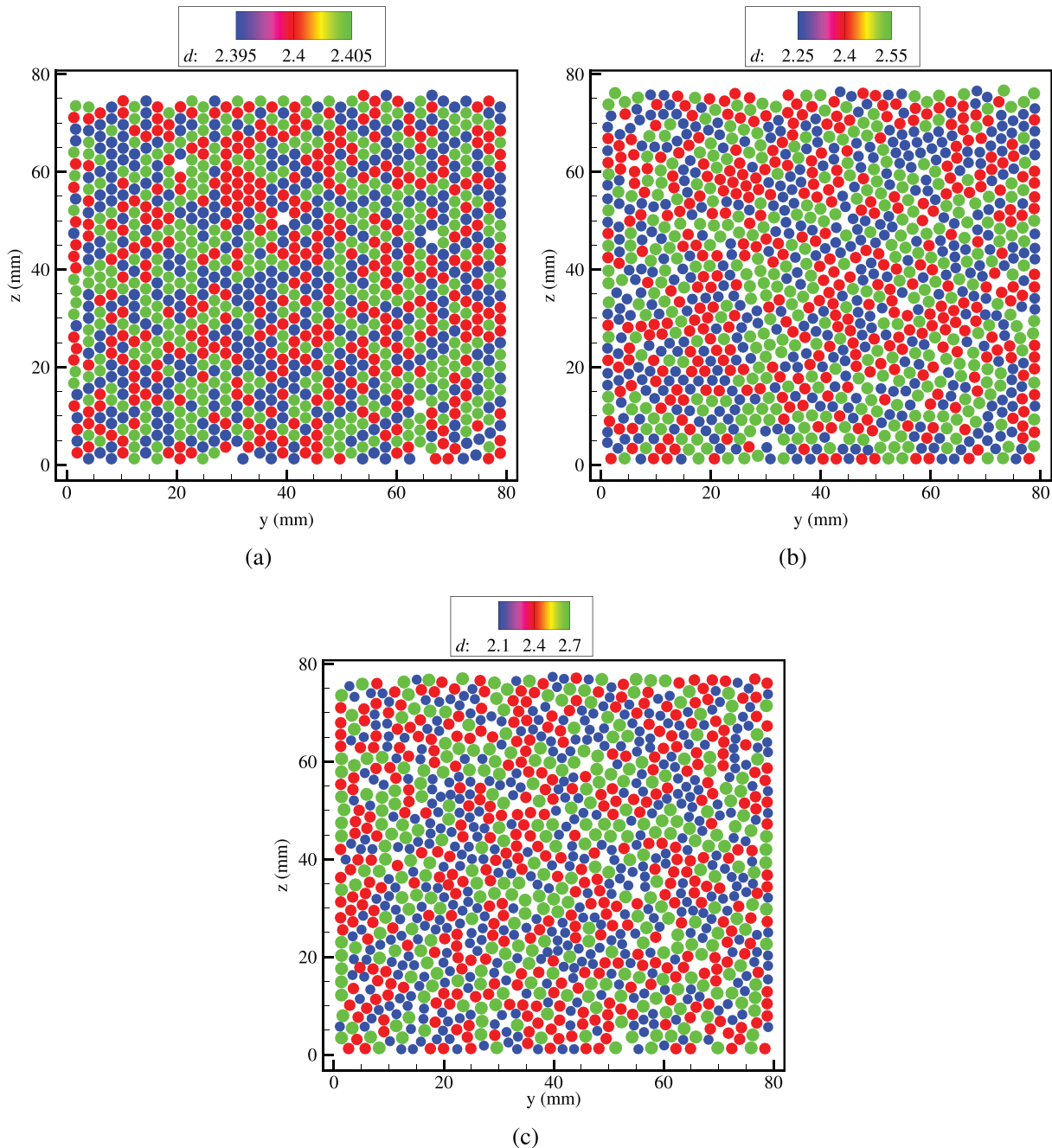


Fig. 26. The distribution of first wall layer spheres on back wall for polydisperse packing with polydispersity of (a) 0.0021 (SP9), (b) 0.063 (SP15), (c) 0.125 (SP17). [Color online].

assembly increases the randomness of the packing, thereby decreasing the packing fraction of the assembly.

6. Summary and conclusions

In this work, packing of mono-sized and polydisperse spherical particles in a slender prismatic container assisted by one-dimensional vibration is simulated. The simulation results are in good agreement with the experimental findings. Further, the transient response of the mono-sized assembly during the vibration process is studied. Within the range of amplitude and frequency of vibration considered, vibration is found to increase the orderliness of particle packing, which leads to the close packing of particles. However, with higher vibrational energy, disturbances in the order structure arise because of

highly excited particles, leading to a lower packing density. The influence of the inclination of the container, during filling, on the packing structure is studied. The packing structure is found to be independent of the orientation or the inclination of the container. However, inclined containers are most beneficial in the applications requiring complete filling of the containers. Granular assemblies, when subjected to vertical vibration, are found to form densely packed assemblies as compared to horizontal vibration. This effect may be attributed to the space available for particle mobility and the assistance of gravity. Further, the influence of X/d_m ratio and λ in polydisperse granular assembly on the packing structure is studied. Higher X/d_m ratio for a granular assembly leads to the formation of the zone with a random arrangement of particles. This is due to the decrease in the influence of walls on the particle arrangement with the increase in the X/d_m ratio. The

effect of the wall is limited to 4d-6d layers of particles independent of the X/d_m ratio. Therefore, with the increase in the X/d_m ratio, an increase in particle layers leads to the increase in the formation of zones of random arrangement of particles. Particle mobility increases with the increase in polydispersity ($\lambda \approx 0.125$). Due to the increase in particle mobility, the randomness in the particle arrangement increases. Therefore, with the increase in polydispersity (λ), there is an increase in the zones of random arrangement of particles. This work shows that the DEM simulations can capture the realistic packing structure of granular assemblies obtained through various filling strategies and geometric variations.

Declaration of Competing Interest

The authors declare that they have no conflict of interest.

Acknowledgements

The authors thankfully acknowledge the resources provided by the High Performance Computing Environment (HPCE), Indian Institute of Technology (IIT) Madras. The authors also acknowledge the generous financial support from IIT Madras under the institutes of eminence (IoE) scheme funded by Ministry of Education, Government of India.

References

- [1] Y. Gan, Thermo-Mechanics of Pebble Beds in Fusion Blankets, Ph.D. thesis University of Karlsruhe, Germany, 2008.
- [2] O. Birkholz, Y. Gan, M. Kamlah, Modeling the effective conductivity of the solid and the pore phase in granular materials using resistor networks, *Powder Technol.* 351 (2019) 54–65.
- [3] M. Rady, Thermal performance of packed bed thermal energy storage units using multiple granular phase change composites, *Appl. Energy* 86 (2009) 2704–2720.
- [4] J. Reimann, L. Boccaccini, M. Enoeda, A. Ying, Thermomechanics of solid breeder and Be pebble bed materials, *Fusion Eng. Des.* 61 (2002) 319–331.
- [5] J. Reimann, B. Fretz, S. Pupeschi, Thermo-mechanical screening tests to qualify beryllium pebble beds with non-spherical pebbles, *Fusion Eng. Des.* 98 (2015) 1851–1854.
- [6] Y. Gan, M. Kamlah, Thermo-mechanical analysis of pebble beds in HELICA mock-up experiments, *Fusion Eng. Des.* 83 (2008) 1313–1316.
- [7] M. Moscardini, Y. Gan, R. Annabattula, M. Kamlah, A discrete element method to simulate the mechanical behavior of ellipsoidal particles for a fusion breeding blanket, *Fusion Eng. Des.* 121 (2017) 22–31.
- [8] Y. Gan, M. Kamlah, Discrete element modelling of pebble beds: with application to uniaxial compression tests of ceramic breeder pebble beds, *J. Mech. Phys. Solid* 58 (2010) 129–144.
- [9] A. Ying, J. Reimann, L. Boccaccini, M. Enoeda, M. Kamlah, R. Knitter, Y. Gan, J.G. van der Laan, L. Maggielsen, P. Di Maio, et al., Status of ceramic breeder pebble bed thermo-mechanics R&D and impact on breeder material mechanical strength, *Fusion Eng. Des.* 87 (2012) 1130–1137.
- [10] Y. Gan, F. Hernandez, D. Hanaor, R. Annabattula, M. Kamlah, P. Pereslavtsev, Thermal discrete element analysis of EU solid breeder blanket subjected to neutron irradiation, *Fus. Sci. Technol.* 66 (2014) 83–90.
- [11] S. Pupeschi, M. Moscardini, Y. Gan, R. Knitter, M. Kamlah, Cyclic behavior of ceramic pebble beds under mechanical loading, *Fusion Eng. Des.* 134 (2018) 11–21.
- [12] H. Bindra, P. Bueno, J.F. Morris, R. Shinnar, Thermal analysis and energy evaluation of packed bed thermal storage systems, *Appl. Therm. Eng.* 52 (2013) 255–263.
- [13] R. Annabattula, Y. Gan, S. Zhao, M. Kamlah, Mechanics of a crushable pebble assembly using discrete element method, *J. Nucl. Mater.* 430 (2012) 90–95.
- [14] R.K. Annabattula, M. Kolb, Y. Gan, R. Rolli, M. Kamlah, Size-dependent crush analysis of lithium orthosilicate pebbles, *Fus. Sci. Technol.* 66 (2014) 136–141.
- [15] R.K. Desu, Y. Gan, M. Kamlah, R.K. Annabattula, Mechanics of binary crushable granular assembly through discrete element method, *Nucl. Mater. Energy* 9 (2016) 237–241.
- [16] P. Wu, X. Dong, C. Gu, S. Ge, Z. Su, Y. Lu, C. Guo, G. Shao, Y. Zhong, A. Liu, Designation of a nano- Fe_3O_4 based composite electrode with long cycle life for lithium-ion batteries, *ChemElectroChem* 6 (2019) 3606–3614.
- [17] R.K. Desu, A.R. Peeketi, R.K. Annabattula, Influence of bed conditions on the effective thermal conductivity of ceramic breeder pebble beds using thermal DEM (TDEM), *Fusion Eng. Des.* 159 (2020) 111767.
- [18] W. Dai, D. Hanaor, Y. Gan, The effects of packing structure on the effective thermal conductivity of granular media: a grain scale investigation, *Int. J. Therm. Sci.* 142 (2019) 266–279.
- [19] H. Zhang, H. Guo, M. Ye, Z. Li, H. Huang, Investigation on the packing behaviors and mechanics of Li_4SiO_4 pebble beds by discrete element method, *Fusion Eng. Des.* 125 (2017) 551–555.
- [20] R.K. Annabattula, Y. Gan, M. Kamlah, Mechanics of binary and polydisperse spherical pebble assembly, *Fusion Eng. Des.* 87 (2012) 853–858.
- [21] D. Mandal, D. Sathiyamoorthy, M. Vinjamur, Void fraction and effective thermal conductivity of binary particulate bed, *Fusion Eng. Des.* 88 (2013) 216–225.
- [22] K. Dong, R. Yang, R. Zou, A. Yu, Role of interparticle forces in the formation of random loose packing, *Phys. Rev. Lett.* 96 (2006) 145505.
- [23] P.A. Cundall, O.D. Strack, A discrete numerical model for granular assemblies, *Geotechnique* 29 (1979) 47–65.
- [24] R.K. Desu, A. Moorthy, R.K. Annabattula, DEM simulation of packing mono-sized pebbles into prismatic containers through different filling strategies, *Fusion Eng. Des.* 127 (2018) 259–266.
- [25] Y. Gan, M. Kamlah, J. Reimann, Computer simulation of packing structure in pebble beds, *Fusion Eng. Des.* 85 (2010) 1782–1787.
- [26] B. Gong, Y. Feng, H. Liao, X. Wu, S. Wang, X. Wang, K. Feng, Numerical investigation of the pebble bed structures for HCCB TBM, *Fusion Eng. Des.* 136 (2018) 1444–1451.
- [27] H. Suikkanen, J. Ritvanen, P. Jalali, R. Kyrki-Rajamäki, Discrete element modelling of pebble packing in pebble bed reactors, *Nucl. Eng. Des.* 273 (2014) 24–32.
- [28] Q. Qian, X. An, H. Zhao, K. Dong, Y. Wu, H. Fu, H. Zhang, X. Yang, Particle scale study on the crystallization of mono-sized cylindrical particles subject to vibration, *Powder Technol.* 352 (2019) 470–477.
- [29] Y. Wu, X. An, A. Yu, DEM simulation of cubical particle packing under mechanical vibration, *Powder Technol.* 314 (2017) 89–101.
- [30] B. Zhao, X. An, Y. Wang, H. Zhao, L. Shen, X. Sun, R. Zou, Packing of different shaped tetrahedral particles: DEM simulation and experimental study, *Powder Technol.* 360 (2020) 21–32.
- [31] K. Dong, C. Wang, A. Yu, A novel method based on orientation discretization for discrete element modeling of non-spherical particles, *Chem. Eng. Sci.* 126 (2015) 500–516.
- [32] J. Gan, A. Yu, DEM study on the packing density and randomness for packing of ellipsoids, *Powder Technol.* 361 (2020) 424–434.
- [33] X. Wang, J. Gong, A. An, K. Zhang, Z. Nie, Random generation of convex granule packing based on weighted voronoi tessellation and cubic-polynomial-curve fitting, *Comput. Geotech.* 113 (2019) 103088.
- [34] X. Wang, Z. Liang, Z. Nie, J. Gong, Stochastic numerical model of stone-based materials with realistic stone-inclusion features, *Constr. Build. Mater.* 197 (2019) 830–848.
- [35] X. Wang, Z. Nie, J. Gong, Z. Liang, Random generation of convex aggregates for DEM study of particle shape effect, *Constr. Build. Mater.* 268 (2021) 121468.
- [36] L. Zhao, S. Zhang, D. Huang, X. Wang, Y. Zhang, 3D shape quantification and random packing simulation of rock aggregates using photogrammetry-based reconstruction and discrete element method, *Constr. Build. Mater.* 262 (2020) 119986.
- [37] T. Jia, Y. Zhang, J. Chen, Y. He, Dynamical simulation of granular packing of fine cohesive particles with different size distributions, *Powder Technol.* 218 (2012) 76–85.
- [38] A. Vijayan, R.K. Annabattula, Effect of particle flow dynamics on the fabric evolution in spherical granular assemblies filled under gravity, *Powder Technol.* 356 (2019) 909–919.
- [39] A. Vijayan, Y. Gan, R.K. Annabattula, Evolution of fabric in spherical granular assemblies under the influence of various loading conditions through DEM, *Granul. Matter* 22 (2020) 1–15.
- [40] Z. Xie, Y. Shen, K. Takabatake, A. Yamaguchi, M. Sakai, Coarse-grained DEM study of solids sedimentation in water, *Powder Technol.* 361 (2020) 21–32.
- [41] P.M. Widartimingsih, Y. Mori, K. Takabatake, C.-Y. Wu, K. Yokoi, A. Yamaguchi, M. Sakai, Coarse graining DEM simulations of a powder die-filling system, *Powder Technol.* 371 (2020) 83–95.
- [42] K. Takabatake, Y. Mori, J.G. Khinast, M. Sakai, Numerical investigation of a coarse-grain discrete element method in solid mixing in a spouted bed, *Chem. Eng. J.* 346 (2018) 416–426.
- [43] M. Moscardini, Y. Gan, S. Pupeschi, M. Kamlah, Discrete element method for effective thermal conductivity of packed pebbles accounting for the smoluchowski effect, *Fusion Eng. Des.* 127 (2018) 192–201.
- [44] A.R. Peeketi, M. Moscardini, A. Vijayan, Y. Gan, M. Kamlah, R.K. Annabattula, Effective thermal conductivity of a compacted pebble bed in a stagnant gaseous environment: an analytical approach together with DEM, *Fusion Eng. Des.* 130 (2018) 80–88.
- [45] A.R. Peeketi, M. Moscardini, S. Pupeschi, Y. Gan, M. Kamlah, R.K. Annabattula, Analytical estimation of the effective thermal conductivity of a granular bed in a stagnant gas including the smoluchowski effect, *Granul. Matter* 21 (2019) 93.
- [46] J. Martis, R.K. Annabattula, A semi-analytical model for the effective thermal conductivity of a multi-component polydisperse granular bed, *Granul. Matter* 19 (2017) 84.
- [47] H. Chen, Q. Wei, Y. Zhang, F. Chen, Y. Shi, W. Yan, Powder-spreading mechanisms in powder-bed-based additive manufacturing: experiments and computational modeling, *Acta Mater.* 179 (2019) 158–171.
- [48] J. Reimann, J. Vicente, E. Brun, C. Ferrero, Y. Gan, A. Rack, X-ray tomography investigations of mono-sized sphere packing structures in cylindrical containers, *Powder Technol.* 318 (2017) 471–483.
- [49] V. Ratnaswamy, A. Rosato, D. Blackmore, X. Tricoche, N. Ching, L. Zuo, Evolution of solids fraction surfaces in tapping: simulation and dynamical systems analysis, *Granul. Matter* 14 (2012) 163–168.
- [50] Y. Nahmud-Molinari, J. Ruiz-Suarez, Epitaxial growth of granular single crystals, *Phys. Rev. Lett.* 89 (2002) 264302.
- [51] N. Zhang, A.D. Rosato, Experiments and simulations on vibration induced densification of bulk solids, *KONA Powd. Part. J.* 24 (2006) 93–103.
- [52] R. Al-Raoush, K.A. Alsibili, Distribution of local void ratio in porous media systems from 3d x-ray microtomography images, *Phys. A: Stat. Mech. Appl.* 361 (2006) 441–456.
- [53] A. Yu, X. An, R. Zou, R. Yang, K. Kendall, Self-assembly of particles for densest packing by mechanical vibration, *Phys. Rev. Lett.* 97 (2006) 265501.

- [54] J. Reimann, R. Pieritz, C. Ferrero, M. Di Michiel, R. Rolli, X-ray tomography investigations on pebble bed structures, *Fusion Eng. Des.* 83 (2008) 1326–1330.
- [55] X. An, R. Yang, R. Zou, A. Yu, Effect of vibration condition and inter-particle frictions on the packing of uniform spheres, *Powder Technol.* 188 (2008) 102–109.
- [56] X. An, C. Li, R. Yang, R. Zou, A. Yu, Experimental study of the packing of mono-sized spheres subjected to one-dimensional vibration, *Powder Technol.* 196 (2009) 50–55.
- [57] A.D. Rosato, O. Dybenko, D.J. Horntrop, V. Ratnaswamy, L. Kondic, Microstructure evolution in density relaxation by tapping, *Phys. Rev. E* 81 (2010), 061301.
- [58] X. An, R. Yang, K. Dong, A. Yu, DEM study of crystallization of mono-sized spheres under mechanical vibrations, *Comput. Phys. Commun.* 182 (2011) 1989–1994.
- [59] R.A. Pieritz, J. Reimann, C. Ferrero, 3D tomography analysis of the inner structure of pebbles and pebble beds, *Adv. Eng. Mater.* 13 (2011) 145–155.
- [60] J. Reimann, E. Brun, C. Ferrero, J. Vicente, Pebble bed structures in the vicinity of concave and convex walls, *Fusion Eng. Des.* 98 (2015) 1855–1858.
- [61] R. Amirifar, K. Dong, Q. Zeng, X. An, Self-assembly of granular spheres under one-dimensional vibration, *Soft Matter* 14 (2018) 9856–9869.
- [62] W. Dai, J. Reimann, D. Hanaor, C. Ferrero, Y. Gan, Modes of wall induced granular crystallisation in vibrational packing, *Granul. Matter* 21 (2019) 1–16.
- [63] R. Amirifar, K. Dong, Q. Zeng, X. An, Bimodal self-assembly of granular spheres under vertical vibration, *Soft Matter* 15 (2019) 5933–5944.
- [64] J. Reimann, J. Vicente, C. Ferrero, A. Rack, Y. Gan, 3D tomography analysis of the packing structure of spherical particles in slender prismatic containers, *Int. J. Mater. Res.* 111 (2020) 65–77.
- [65] R.F. Benenati, C.B. Brosilow, Void fraction distribution in beds of spheres, *J. AIChE* 8 (1962) 359–363.
- [66] F. Hernández, P. Pereslavtsev, Q. Kang, P. Norajitra, B. Kiss, G. Nádas, O. Bitz, A new HCPB breeding blanket for the EU DEMO: evolution, rationale and preliminary performances, *Fusion Eng. Des.* 124 (2017) 882–886.
- [67] A. Abou-Sena, H. Neuberger, T. Ihli, Experimental investigation on the possible techniques of pebbles packing for the hcpb test blanket module, *Fus. Eng. Des.* 84 (2009) 355–358.
- [68] S. Hekmat, G. Molaeimanesh, Hybrid thermal management of a li-ion battery module with phase change material and cooling water pipes: An experimental investigation, *Appl. Therm. Eng.* 166 (2020) 114759.
- [69] S. Panchal, I. Dincer, M. Agelin-Chaab, R. Fraser, M. Fowler, Experimental and theoretical investigation of temperature distributions in a prismatic lithium-ion battery, *Int. J. Therm. Sci.* 99 (2016) 204–212.
- [70] L. Sheng, L. Su, H. Zhang, Y. Fang, H. Xu, W. Ye, An improved calorimetric method for characterizations of the specific heat and the heat generation rate in a prismatic lithium ion battery cell, *Energy Convers. Manag.* 180 (2019) 724–732.
- [71] C. Kloss, C. Goniva, A. Hager, S. Amberger, S. Pirker, Models, algorithms and validation for opensource DEM and CFD-DEM, *Prog. Comput. Fluid Dyn.* 12 (2012) 140–152.
- [72] E. Brun, J. Vicente, F. Topin, R. Occelli, imorph: A 3d Morphological Tool to Fully Analyze all Kind of Cellular Materials (in cellmet'08), Dresden, Germany 2008.
- [73] MATLAB, 9.7.0.1190202 (R2019b), The MathWorks Inc, Natick, Massachusetts, 2018.